

THE *s*-PROCESS IN ROTATING ASYMPTOTIC GIANT BRANCH STARS

FALK HERWIG

Department of Physics and Astronomy, University of Victoria, 3800 Finnerty Road, Victoria, BC V8P 1A1, Canada;
fherwig@uvastro.phys.uvic.ca

NORBERT LANGER

Astronomical Institute, Universiteit Utrecht, P.O. Box 80000, NL-3508 TA Utrecht, Netherlands;
n.langer@astro.uu.nl

AND

MARIA LUGARO

Institute of Astronomy, University of Cambridge, Madingley Road, Cambridge CB3 0HA, UK;
mal@ast.cam.ac.uk

Received 2002 November 26; accepted 2003 May 6

ABSTRACT

We model the nucleosynthesis during the thermal pulse phase of a rotating, solar metallicity, asymptotic giant branch (AGB) star of $3 M_{\odot}$, which was evolved from a main-sequence model rotating with 250 km s^{-1} at the stellar equator. Rotationally induced mixing during the thermal pulses produces a layer ($\sim 2 \times 10^{-5} M_{\odot}$) on top of the CO core where large amounts of protons and ^{12}C coexist. With a postprocessing nucleosynthesis and mixing code, we follow the abundance evolution in this layer, in particular that of the neutron source ^{13}C and of the neutron poison ^{14}N . In our AGB model mixing persists during the entire interpulse phase because of the steep angular velocity gradient at the core-envelope interface, thereby spreading ^{14}N over the entire ^{13}C -rich part of the layer. We follow the neutron production during the interpulse phase and find a resulting maximum neutron exposure of $\tau_{\text{max}} = 0.04 \text{ mbarn}^{-1}$, which is too small to produce any significant *s*-process. In parametric models, we then investigate the combined effects of diffusive overshooting from the convective envelope and rotationally induced mixing. Just adding the overshooting and leaving the rotational mixing unchanged results in a small maximum neutron exposure (0.03 mbarn^{-1}). Models with overshoot and weaker interpulse mixing—as perhaps expected from more slowly rotating stars—yield larger neutron exposures. In a model with overshooting without any interpulse mixing a neutron exposure of up to 0.72 mbarn^{-1} is obtained, which is larger than required by observations. We conclude that the incorporation of rotationally induced mixing processes has important consequences for the production of heavy elements in AGB stars. While through a distribution of initial rotation rates, it may lead to a natural spread in the neutron exposures obtained in AGB stars of a given mass in general—as appears to be required by observations—it may moderate the large neutron exposures found in models with diffusive overshoot in particular. Our results suggest that both processes, diffusive overshoot and rotational mixing, may be required to obtain a consistent description of the *s*-process in AGB stars that fulfills all observational constraints. Finally, we find that mixing due to rotation within our current framework does increase the production of ^{15}N in the partial mixing zone. However, this increase is not large enough to boost the production of fluorine to the level required by observations.

Subject headings: nuclear reactions, nucleosynthesis, abundances — stars: AGB and post-AGB — stars: evolution — stars: interiors — stars: rotation

1. INTRODUCTION

Trans-iron elements are mainly made by neutron capture reactions on ^{56}Fe seed nuclei. Two processes have been distinguished according to the neutron density at the production site. In the case of the *r*-process, the *n*-densities are high ($N_n > 10^{20} \text{ cm}^{-3}$), and the timescale of successive *n*-capture reactions on heavy isotopes is faster than the β -decay timescale. Such a sudden high-density neutron burst creates isotopes far away from the valley of β -stability in the chart of nuclides, which successively decay back to the stable isotopes. In contrast, the *s*-process is characterized by lower neutron densities ($N_n \lesssim 10^{10} \text{ cm}^{-3}$). Neutron captures are generally followed by β -decays since unstable isotopes on the *s*-process path have typical lifetimes of the order of hours. In some cases, however, the unstable isotopes involved have longer lifetimes, and, depending on the neutron density and temperature conditions, *branchings* can

be open on the *s*-process path, leading to the production of neutron-rich isotopes (see Clayton 1968 for an introduction to the *s*-process).

In asymptotic giant branch (AGB) stars, recurrent He-shell flashes (thermal pulses [TPs]) drive a convective zone that temporarily covers the whole region between the H-burning and the He-burning shells (intershell). Here partial He burning produces a high mass fraction (> 0.25) of ^{12}C , and the chain $^{14}\text{N}(\alpha, \gamma)^{18}\text{F}(\beta^+, \nu)^{18}\text{O}(\alpha, \gamma)^{22}\text{Ne}$ starting on the abundant ^{14}N from the H-burning ashes produces a relatively large amount of ^{22}Ne (mass fraction $\simeq 0.02$). The $^{22}\text{Ne}(\alpha, n)^{25}\text{Mg}$ reaction as a neutron source for the *s*-process was suggested by Cameron (1960). Temperatures above $3 \times 10^8 \text{ K}$ are required for that reaction to release a significant amount of neutrons. Stellar models showed that such high temperatures are achieved in intermediate-mass ($M_{\text{ZAMS}}/M_{\odot} > 4$) AGB stars, which were hence proposed as the main site for the production of *s*-process elements

belonging to the solar main component, i.e., $90 < A < 204$ (Iben 1975; Truran & Iben 1977). However, the neutron density produced by ^{22}Ne burning in TPs is rather high (above 10^{11} cm^{-3} for $T = 3.5 \times 10^8 \text{ K}$). This leads to excesses in the neutron-rich nuclides produced by branchings, for example, ^{86}Kr , ^{87}Rb , and ^{96}Zr (see, e.g., Despain 1980), in contrast with the great majority of the observations of *s*-process-enhanced stars such as MS, S, and C stars. In S and C stars the Rb/Sr ratio is typically much lower than solar (Lambert et al. 1995; Abia et al. 2001), indicating a low neutron density at the *s*-process site. Also, the Rb abundances observed in 10 AGB members of the massive Galactic globular cluster ω Centauri indicate a low neutron density for the *s*-process (Smith et al. 2000). Lambert et al. (1995) reported the zirconium isotopic abundance obtained by spectroscopic observations of the ZrO band heads in M, MS, and S stars and found no evidence of an excess of the neutron-rich ^{96}Zr , which can be produced in great amount by the *s*-process when the neutron density exceeds $\sim 5 \times 10^8 \text{ n cm}^{-3}$. Another problem is that the activation of the $^{22}\text{Ne}(\alpha, n)^{25}\text{Mg}$ is expected to produce an excess of ^{25}Mg in stars enriched in *s*-process elements. Instead, these stars typically have magnesium isotopic abundances in solar proportion (see, e.g., Smith & Lambert 1986; McWilliam & Lambert 1988). Also, other types of observations tend to exclude AGB stars of intermediate mass as the main *s*-process site. Observations mainly show that MS, S, and C stars have low luminosity (Frogel, Mould, & Blanco 1990) and hence low mass. Feast (1989) performed a study of the kinematics of peculiar red giants, including S, SC, and C stars. On the basis of 183 S-SC stars and 463 C stars, he estimated their mean masses to be 1.3 and $1.6 M_{\odot}$, respectively, although this estimate needs to be improved. In summary, the observational evidence and the

current state of AGB evolution models suggest that the major nuclear production site of the *s*-process is low-mass AGB stars.

In low-mass AGB stars the temperature in the intershell is not high enough to burn a significant amount of ^{22}Ne . The $^{13}\text{C}(\alpha, n)^{16}\text{O}$ neutron source reaction, which was suggested by Greenstein (1954) and Cameron (1955) and is activated at lower temperatures ($\sim 0.9 \times 10^8 \text{ K}$), is expected to play the major role (Iben & Renzini 1982; Gallino et al. 1988; Käppeler et al. 1990). However, an amount of ^{13}C higher than that present in the H-burning ashes is needed to reproduce the observed enhancements of heavy elements. In order to form a sufficient amount of ^{13}C , it is hence speculated that some protons mix into the ^{12}C -rich intershell (see Busso, Gallino, & Wasserburg 1999 for a general review of the *s*-process in AGB stars).

In recent years a picture of the *s*-process based on these results has emerged (Gallino et al. 1998), and it is summarized in Figure 1. The He flash convection zone homogenizes the intershell region, and ^{12}C produced in the He-burning shell is mixed up to just below the location of the H-burning shell. The dashed line in Figure 1 indicates that, after the convective pulse is extinguished, the convectively unstable envelope may extend down into H-free layers of the intershell region. This phenomenon allows processed intershell material to be carried into the envelope and hence to the stellar surface (*third dredge-up*). At the end of third dredge-up a layer is created where the H-rich envelope directly neighbors the ^{12}C -rich intershell. This layer is a favorable region for the formation of a zone where ^{12}C and protons are partially mixed. As the temperature increases in the region a pocket of ^{13}C forms by proton captures on ^{12}C . Subsequently, the ^{13}C serves as a neutron donor via the reaction $^{13}\text{C}(\alpha, n)^{16}\text{O}$, which is activated during the

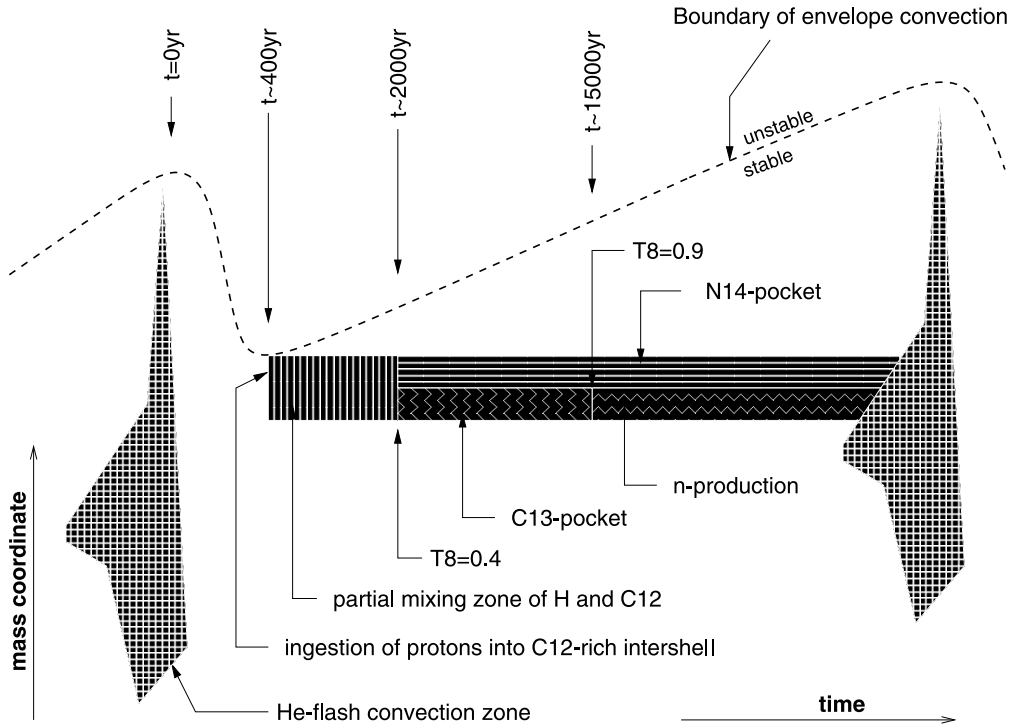


FIG. 1.—Schematic representation of the *s*-process in the interpulse phase of TP-AGB stars in a space-time diagram. The ordinate covers the mass range between the H- and He-burning shells (intershell). The time marks represent a rough estimate.

following interpulse phase at $T \sim 9 \times 10^7$ K so that neutrons are released under radiative conditions (Straniero et al. 1995). Typically, the s -process occurs on a timescale of several tens of thousands years and before the onset of the following TP. In the convective pulse the ^{22}Ne neutron source is only marginally activated.

It is most reasonable to assume that the $\text{H}/^{12}\text{C}$ ratio in the partial mixing zone varies somehow continuously from a few hundred in the envelope to zero in the intershell. Then one finds in the top layers of the partial mixing zone another pocket made of ^{14}N , which forms where the $\text{H}/^{12}\text{C}$ ratio is larger than where the ^{13}C pocket forms. Without further mixing the partial mixing layer is strictly stratified during the interpulse period: as shown in Figure 1, the two pockets coexist without much interaction. During the interpulse phase the temperature does not reach values required for the $^{14}\text{N}(\alpha, \gamma)^{18}\text{F}$ reaction. The ^{14}N pocket is engulfed into the following He flash convection zone, where it might slightly contribute to the production of ^{22}Ne .

Stellar models that use a standard treatment of convective mixing cannot produce the ^{13}C pocket because extra mixing processes are required to allow a small amount of protons to enter the ^{12}C -rich region. Gallino et al. (1998) and following studies by that group and Goriely & Mowlavi (2000) have studied the s -process by assuming a certain proton profile extending into the ^{12}C -rich region without relating explicitly to a specific physical process. In these studies it was implicitly assumed that any subsequent alterations of the abundances in the partial mixing zone are due to nucleosynthesis only and that no mixing takes place during the interpulse phase after the initial formation of the partial mixing zone. In this way it was possible to develop a fairly good understanding of the s -process nucleosynthesis in the ^{13}C pocket. For example, it was shown that many observations are reproduced with models in which the neutron exposure in the ^{13}C pocket is up to $\simeq 0.4 \text{ mbarn}^{-1}$ at solar metallicity. In order to account for the observed s -process overabundances, the partial mixing zone needs to have a mass of 10^{-4} to $10^{-3} M_{\odot}$. These s -process models with an assumed H profile for the partial mixing zone can account for many of the overall observed properties of the s -process.

However, to explain the observed s -process signature in AGB stars as a function of metallicity, the s -process model described above requires that stars of the same mass and metallicity have different neutron exposures due to the ^{13}C neutron source during the AGB interpulse phase (Busso et al. 2001). A mixing process for the formation and evolution of this neutron source that allows for some *spread in the efficiency of producing neutrons* seems to be necessary. Van Winckel & Reyniers (2000) arrive at the same conclusion from observations of weakly metal-poor, post-AGB stars with a $21 \mu\text{m}$ feature. In these objects the s -process element signatures are easier to measure than in the cool progenitor AGB stars. Also, the spread in the Pb abundance observed in very low-metallicity stars (see, e.g., Van Eck et al. 2003) could fit into the current s -process model only if there is a spread in the number of neutrons available in the pocket for the s -process. Such a spread in the efficiency of the ^{13}C neutron source is also required to explain the measurements of isotopic ratios in single presolar silicon carbide grains (SiC) recovered from pristine carbonaceous meteorites (Zinner 1998). The majority of these grains are believed to have formed in the circumstellar dusty envelopes surrounding carbon stars. The main evidence for this comes from mea-

surements of aggregates of SiC that have shown a very strong signature of the s -process in the heavy elements present in trace (see, e.g., Gallino, Busso, & Lugaro 1997). Nicolussi et al. (1997, 1998a, 1998b) and Savina et al. (2003) performed measurements of the composition of Sr, Zr, Mo, and Ba in single SiC grains. Isotopic ratios that are sensitive to the efficiency of the ^{13}C neutron source have been found to show a large spread within the single-grain data. This can be explained if SiC grains were formed in a multiplicity of low-mass AGB stars with a range of neutron exposures in the ^{13}C pocket. These isotopic ratios are those involving nuclei with a very low neutron capture cross section, such as nuclei with numbers of neutrons equal or near to nuclear magic numbers, i.e., $^{88}\text{Sr}/^{86}\text{Sr}$, $^{90,91,92}\text{Zr}/^{94}\text{Zr}$, and $^{138}\text{Ba}/^{136}\text{Ba}$. A detailed analysis of SiC grain data indicated that a spread of the order of 5 is necessary in the neutron exposure for a given mass and metallicity (Lugaro et al. 2003a). These new insights are specifically important for constraining the physical processes that are responsible for the partial mixing between envelope and core and thereby lead to the formation of the ^{13}C neutron source. Moreover, neutron capture elements are in general becoming an increasingly important target of stellar observations, for example, of IR observations in planetary nebulae (Dinerstein 2001).

The open problem addressed in this paper is the role of rotational mixing. Rotation is an effect that has to be taken into account when studying stellar evolution and nucleosynthesis. Most F stars, which are the main-sequence progenitors of low-mass AGB stars, show rotational velocities of a few hundred kilometers per second (Royer et al. 2002; Royer, Zorec, & Frémat 2003). The importance of rotation as a physical process in AGB stars is not restricted to mixing and nucleosynthesis. Rotation in stars during their late evolutionary phase possibly drives the shaping of bipolar proto-planetary nebulae. According to the interacting stellar winds model (Kwok 1982; Balick 1987), a fast ionized stellar wind interacts with an equatorially dense AGB circumstellar envelope that could be the result of inhomogeneities associated with rotation. This model can qualitatively explain the presence of sharp radial structures and the wide variety of shapes found in planetary nebulae (see also Icke, Balick, & Frank 1992). Reimers, Dorfi, & Höfner (2000) find that elliptical or weakly bipolar planetary nebula shapes can result from dust-driven winds of rotating AGB stars. Soker (2001) considers the possibility that increased rotation in an AGB envelope may result from swallowing another celestial body, like a companion star in a binary system or an orbiting planet. Indeed, this hypothesis gains support from the recent discovery of many extrasolar planets and the detection of water vapor around evolved AGB stars, possibly due to the presence of comets (Melnick et al. 2001). García-Segura, Langer, & Różyczka (1999) present hydrodynamical models in which an equatorial-density enhancement originates around an intermediate-mass single AGB star with a fast rotating core that can spin up the extended envelope during mixing events associated with the He-shell flashes.

Langer et al. (1999) evolved a $3 M_{\odot}$ stellar model from the main sequence to the AGB phase, including the effects of rotation on the stellar structure and mixing. They found that rotationally induced mixing at the core-envelope interface after a TP could be responsible for the formation of the partial mixing zone that hosts a ^{13}C pocket and subsequent s -process nucleosynthesis. They also found that mixing in

the partial mixing layer continues throughout the entire interpulse phase. In this paper we investigate mixing and the s -process at the core-envelope interface of this stellar model with rotation. We also present a comparison with models including mixing due to hydrodynamic overshooting, as well as parametric models that further illustrate the effect of slow mixing of the s -process layer during the interpulse period.

In the current model the s -process occurs in every interpulse-pulse cycle from when third dredge-up starts until the end of the AGB evolution. Several stellar parameters that are important for the computation of the s -process, e.g., the mass of the intershell, the temperature at the base of the convective shell, the overlapping factor between subsequent pulses, and the third dredge-up, are different at each interpulse-pulse cycle. Detailed s -process calculations, such as those of Gallino et al. (1998), take into account these effects. However, the features of the ^{13}C pocket are kept the same in each interpulse, and the changes in the temperature are not large enough to affect the modality of the burning of ^{13}C in different interpulses. The only effect is that in detailed calculations the neutron exposure in the pocket slightly decreases with the interpulse number because the amount of s -process material increases in the intershell. We perform simulations of the s -process over only one interpulse period, which in first approximation represents all the interpulse periods. In § 2 we derive the basic properties of the partial mixing zone and interpulse s -process layer from average observational features and simplified AGB evolution properties. We describe the stellar models and the nucleosynthesis code in § 3. Section 4 is devoted to our scheme for the heavy s -process neutron sink. The properties and effects of mixing induced by hydrodynamic overshoot and by rotation are presented in §§ 5 and 6, respectively. Mixing for the s -process is further explored with synthetic models in § 7. The particular problem of the production of ^{19}F is addressed in § 8, and we present a final discussion in § 9.

2. CONSTRAINTS ON THE PROPERTIES OF THE PARTIAL MIXING ZONE

The properties of a partial mixing zone that reproduces the s -process features observed in AGB stars can be studied in detail with models including the effect of many consecutive TPs and neutron exposure events (Gallino et al. 1998; Goriely & Mowlavi 2000). Here we derive some basic constraints on the properties of the s -process zone by following a much simpler approach. We consider two s -process indicators: the index s/s_{\odot} is the overproduction factor of s -process elements with respect to the initial solar value. We have used for this index the average of the production factors of Y and Nd. The index $[\text{hs}/\text{ls}] = [\text{hs}/\text{Fe}] - [\text{ls}/\text{Fe}]$ is the abundance ratio of heavy-to-light s -process elements. We have used $[\text{ls}/\text{Fe}] = \frac{1}{2}([\text{Y}/\text{Fe}] + [\text{Zr}/\text{Fe}])$ and $[\text{hs}/\text{Fe}] = \frac{1}{5}([\text{Ba}/\text{Fe}] + [\text{La}/\text{Fe}] + [\text{Ce}/\text{Fe}] + [\text{Nd}/\text{Fe}] + [\text{Sm}/\text{Fe}])$, where square brackets indicate the logarithmic ratio with respect to the solar ratio. Observationally, the spectroscopic studies of the s -process abundances in evolved low-mass stars of solar metallicity can be summarized as $0 < \log(s_{\text{obs}}/s_{\odot}) < 1$ and $-0.5 < [\text{hs}/\text{ls}] < 0$ (Busso et al. 1995).

The observed overproduction factors in the envelope are related to the overproduction factors in the s -process zone by two dilution factors that result from two subsequent mix-

ing events: the He flash convective mixing and the third dredge-up. Assuming that no significant amount of s -process material is available in the envelope initially and considering only the contribution of the s -process in the interpulse, the abundance of any species in the envelope after third dredge-up events in m identical TP cycles is related to the abundance in the s -process zone (partial mixing zone [PM]) by

$$Y_{\text{env}} = qm Y_{\text{PM}} \frac{M_{\text{PM}} M_{\text{DUP}}}{M_{\text{IS}} M_{\text{env}}}, \quad (1)$$

where M_{DUP} , M_{IS} , and M_{env} are the masses of the dredged-up layer, the intershell zone covered by the He flash convection, and the envelope, respectively. In low-mass AGB stars with core masses of $\sim 0.6 M_{\odot}$ these quantities are of the order of $M_{\text{DUP}} \sim 3 \times 10^{-3} M_{\odot}$, $M_{\text{IS}} \sim 10^{-2} M_{\odot}$, and $M_{\text{env}} \sim 0.5 M_{\odot}$. These masses vary from pulse to pulse and are dependent on the core mass and the treatment of mixing. For example, in the model sequence with rotation $M_{\text{IS}} = 1 \times 10^{-2} M_{\odot}$ at a core mass of $M_c = 0.746 M_{\odot}$ (Langer et al. 1999), while in the sequence with overshooting at all convective boundaries $M_{\text{IS}} = 2.4 \times 10^{-2} M_{\odot}$ at a core mass of $M_c = 0.628 M_{\odot}$ (Herwig 2000). The mass M_{PM} refers to the layer of the partial mixing zone that at the end of the interpulse phase contains s -process material. In models without mixing during the interpulse phase this corresponds to the region of the partial mixing zone where initially $-3 < \log X(\text{H}) < -2$ (Goriely & Mowlavi 2000). In models with mixing during the interpulse, as in the case with rotation, the extent of the partial mixing zone can only be determined at the end of the interpulse when the calculation has yielded the s -process nucleosynthesis and mixing result. The factor q describes the effect of overlapping He flash convection zones in subsequent TPs (see below).

Without resorting to the detailed results of full stellar evolution calculations, we estimate the number m of TPs with dredge-up events that enrich the envelope in a semiempirical way. As we have discussed in § 1, carbon stars are believed to be the result of recurrent third dredge-up events in low-mass stars with initial zero-age main-sequence (ZAMS) masses predominantly in the range $1.5 < M/M_{\odot} < 3$ (see also Groenewegen, van den Hoek, & de Jong 1997). These stars end their lives as white dwarfs with masses in the range $0.57 < M/M_{\odot} < 0.68$, according to the revised stellar initial-final mass relation of Weidemann (2000). In fact, the mass distribution of white dwarfs peaks at or just below $0.60 M_{\odot}$ (Koester, Weidemann, & Schulz 1979; Weidemann & Koester 1984; Bergeron, Saffer, & Liebert 1992; Napiwotzki, Green, & Saffer 1999). This mass distribution is very similar to that of central stars of planetary nebulae (Stasińska, Górny, & Tylenda 1997), which are in the evolution phase between AGB stars and white dwarfs. This means that the majority of carbon stars must have achieved the necessary abundance enrichment through the third dredge-up before or when reaching a core mass of $\sim 0.6 M_{\odot}$. According to the synthetic AGB models of Marigo, Bressan, & Chiosi (1996), significant dredge-up must commence at core masses of $0.58 M_{\odot}$, or even below in some cases, in order to reproduce the carbon star luminosity function (Marigo, Girardi, & Bressan 1999). Therefore, the relevant chemical enrichment of AGB stars typically occurs within an effective core mass growth of about $\Delta M_{\text{cg}} = 0.02 M_{\odot}$, and maybe up to $0.06 M_{\odot}$ in some cases. For low-mass

TP-AGB stars, the core mass growth per TP is about $\Delta M_{\text{H}} 6 \times 10^{-3} M_{\odot}$, and with a dredge-up parameter of $\lambda = 0.5$, about $m = 7$ ($\Delta M_{\text{cg}} = 0.02$), and possibly up to 20, TPs with dredge-up mixing (if dredge-up starts at $M_c = 0.54 M_{\odot}$, $\Delta M_{\text{cg}} = 0.06$) can be considered to be responsible for the abundance enrichment.

Equation (1) does not take into account that processed heavy elements accumulate in the intershell from one TP to the next because the He flash convection zone is partly overlapping (overlap factor r) with layers that have been swept by the previous He flash convection zone. In the case of nucleosynthesis of a species (s) during the interpulse phase in a partial mixing zone, the production stays roughly constant from TP to TP. The abundance due to such a production is $X_s = X_{\text{PM}} M_{\text{PM}} / M_{\text{IS}}$. The total intershell abundance at the n th TP with third dredge-up is then given by $X_n = X_s + r X_{n-1}$. The number l of TPs needed to approach a 90% level of some asymptotic value for the intershell abundance of species s is given by $l = -1 / \log r$. For $n > l$, it follows that

$$X_n \approx X_s q = X_s \sum_{i=0}^{l-1} r^i. \quad (2)$$

The overlap factor decreases as a function of TP number and also depends on the details of the third dredge-up efficiency. Typically, overlap factors in stellar models decrease from about 0.8 at the earliest TPs to an asymptotic value larger than 0.4. The condition $n > l$ is approximately satisfied for $r \lesssim 0.6$, for which equation (2) returns $q = 2.3$. Other triplets of (r, l, q) are (0.4, 3, 1.6) and (0.8, 11, 4.6). By evaluating equation (1) for the numbers specified above, and with Y_{env} in equation (1) given by using the maximum $\log(s_{\text{obs}}/s_{\odot}) = 1$, we derive a logarithmic expression that relates the s -process overabundance in the PM zone with the mass of that zone:

$$\log M_{\text{PM}} - \log(s_{\text{PM}}/s_{\odot}) + c, \quad (3)$$

where $c = -0.14$ (0, -0.44) for $m = 10$ (7, 20).

In Figure 2 we show the variation of $\log(s_{\text{PM}}/s_{\odot})$ and $[\text{hs}/\text{ls}]_{\text{PM}}$ with the neutron exposure. These trends have been obtained by fully implicit network calculations containing the s -process nucleosynthesis with neutron captures on all isotopes from He to Pb (as in Lugaro et al. 2003b) and all relevant charged particle reactions (see § 3 for reaction rate references). As more neutrons are released, the average s -process overabundance increases. In the current s -process model the partial mixing zone by definition does not extend into the He-burning shell, and therefore the partial mixing zone cannot exceed the mass of the intershell layer. Thus, the mass available for the pocket is $M_{\text{PM}} < 10^{-2} M_{\odot}$. This, together with equation (3) and $m = 10$, requires that $\log(s_{\text{PM}}/s_{\odot}) > 1.86$ and translates into a minimum for τ in the partial mixing zone. In Figure 2 the left shaded part of the diagram with $\tau < 0.2 \text{ mbarn}^{-1}$ is thereby excluded as the predominant region of τ in the partial mixing zone. Values of $\log(s_{\text{PM}}/s_{\odot}) < 1.86$ in that region would require a prohibitively large partial mixing zone ($M_{\text{PM}} > 10^{-2} M_{\odot}$) in order to reproduce the most s -process-enriched stars of solar metallicity with $\log(s_{\text{obs}}/s_{\odot}) = 1$. From $[\text{hs}/\text{ls}]_{\text{obs}} < 0$, the τ -values corresponding to the right shaded area in Figure 2 can be excluded as typical for the s -process. In fact, if the neutron exposure values predominant in the pocket

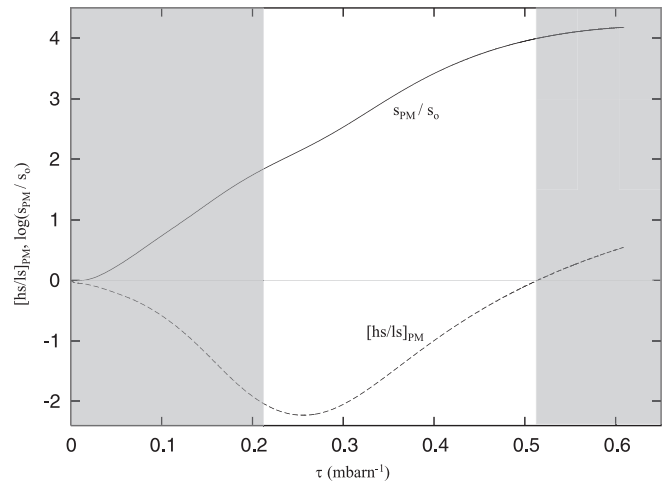


FIG. 2.—The s -process indices $\log(s/s_{\odot})$ and $[\text{hs}/\text{ls}]$ in s -processed material as function of the neutron exposure from a network calculation including all relevant light and heavy elements from H to Pb. The initial ^{13}C mass fraction is 0.03, and neutrons are released by the $^{13}\text{C}(\alpha, n)$ reaction at a constant temperature of 9.8×10^7 K. The neutron exposure corresponding to the shaded areas can be excluded as the dominant contribution in the s -process site (see text). As discussed in the Appendix, the presence of light neutron poison like ^{14}N would limit the neutron exposure that can be achieved, but the relations of τ and the shown indices are only very weakly affected.

exceed $\sim 0.5 \text{ mbarn}^{-1}$, the envelope s -process abundance will show $[\text{hs}/\text{ls}] > 0$. This case is discussed in § 5.3 with an example in Table 1 (see also Lugaro et al. 2003b). To summarize, we estimate the following properties for the partial mixing zone in stars of solar metallicity:

1. The ^{13}C pocket should generate a predominant neutron exposure in the range $\sim 0.2\text{--}0.5 \text{ mbarn}^{-1}$.
2. Using equation (3) and $\log(s_{\text{PM}}/s_{\odot}) = 4$, corresponding to the upper limit of τ , the mass of the partial mixing zone should obey $M_{\text{PM}} > 7 \times 10^{-5} M_{\odot}$ (assuming $m = 10$), in agreement with the detailed studies.

3. STELLAR EVOLUTION AND NUCLEOSYNTHESIS MODELS

Stellar evolution models with rotation are computed in the same way as in Langer et al. (1999). The one-dimensional hydrodynamical stellar evolution code (Langer 1998; Heger, Langer, & Woosley 2000) considers angular momentum, the effect of centrifugal force on the stellar structure, and the following rotationally induced transport mechanisms for angular momentum and chemical species:

TABLE 1
EFFECT OF THE ^{13}C POCKET MASS ON THE s -PROCESS EFFICIENCY AND ABUNDANCE DISTRIBUTION

IP	BM/10	BM/2	BM ^a	BM \times 2
$[\text{ls}/\text{Fe}]$	0.03	0.13	0.23	0.38
$[\text{hs}/\text{Fe}]$	0.06	0.25	0.40	0.61
$[\text{hs}/\text{ls}]$	0.03	0.12	0.17	0.23

^a BM: benchmark ^{13}C pocket corresponding to case with hydrodynamic overshoot with $f = 0.128$.

Eddington-Sweet circulation, Solberg-Høiland and Goldreich-Schubert-Fricke instability, and dynamical and secular shear instability. The μ -gradient, which acts as a barrier for rotationally induced mixing, and the Ledoux criterion for convection and semiconvection are considered. The nuclear energy generation is computed in the operator split approximation with a network including p - p chain, H-burning cycles, and He burning. For comparison, we analyze stellar models with hydrodynamic overshoot of Herwig (2000). These models feature a partial mixing zone of protons and ^{12}C very similar to that assumed for s -process calculations with a parameterized partial mixing zone, as in Goriely & Mowlavi (2000). They assume, however, that overshoot is to some extent present at all convective boundaries. The two processes of rotation and overshoot are considered independently from each other since the stellar evolution models with rotation do not include overshoot and the overshoot models do not include rotation.

The nuclear reactions under consideration for the s -process do not contribute in a significant way to the energy generation in the star. Hence, postprocessing is a valid approximation and a faster and easier-to-handle alternative to recomputing the whole stellar evolution including all the needed nuclear species. An important feature of our rotating-AGB stellar models is a weak and persistent mixing of the partial mixing layer, where the ^{13}C and ^{14}N pockets are located next to each other. The s -process cannot be computed under the assumption of stratification anymore, as done, for example, by Lugaro et al. (2003b). Therefore, we have developed a nucleosynthesis and mixing postprocessing code (SBM6) that solves simultaneously for mixing processes and charged particle nuclear reactions, as well as neutron production and destruction reactions and β -decays. The code uses thermodynamic and mixing properties of the stellar evolution models as input and follows the abundance evolution of the nuclear network described below. In the stellar evolution code with rotation, the time and spatial resolution is determined by the H-burning shell. Grid rezoning after the TP at the core-envelope interface may introduce some numerical diffusion, which can be avoided if the s -process simulation is carried out on a fixed grid beginning right after the formation of the partial mixing zone. In the postprocessing we use a high-resolution, equidistant Lagrangian grid with 400 points to cover our partial mixing layer, which has a mass of $10^{-4} M_{\odot}$. The solution scheme of coupled burning and mixing is fully implicit (Herwig 2001) with adaptive time steps. A Newton-Raphson iteration is accepted as a solution if the corresponding greatest relative correction is less than 10^{-3} for any species at any grid point with a mass fraction $X > 10^{-21}$. This guarantees a numerical precision of 0.1% for any species at each time step and the correct integration of the neutron abundance, which is treated like that of any other species. The neutron density typically encountered during the interpulse ($N_n < 10^7 \text{ n cm}^{-3}$) corresponds to $X(n) < 2 \times 10^{-21}$. In practice the precision for neutrons is much better than 0.1%, even for $X(n) < 10^{-21}$, because the convergence of the set of equations is determined by other species. Because of the fully implicit solution scheme, only a fraction (about 1/100) of the time steps of the evolutionary code need to be computed with the SBM6 code, because in the partial mixing zone the thermodynamic conditions change much more slowly than at the location of the H-burning shell.

For the postprocessing simulations, we have considered the following reactions in the SBM6 code:

1. (p, γ) from the NACRE compilation (Angulo et al. 1999) on ^{12}C , ^{13}C , ^{13}N , ^{14}N , ^{15}N , ^{16}O , ^{17}O , ^{18}O , ^{19}F , ^{20}Ne , ^{21}Ne , ^{22}Ne , ^{22}Na , ^{23}Na , ^{24}Mg , ^{25}Mg (to both $^{26}\text{Al}_g$ and $^{26}\text{Al}_m$), ^{26}Mg , ^{27}Al , ^{28}Si , ^{29}Si , and ^{30}Si ; ^{31}P and $^{26}\text{Al}_g(p, \gamma)$ from Iliadis et al. (2001); $^{14}\text{C}(p, \gamma)$ from Wiescher, Goerres, & Thielemann (1990);
2. (p, α) from NACRE on ^{15}N , ^{17}O , ^{18}O , and ^{19}F ;
3. β -decays have been assumed to follow instantaneously where applicable, except for the β -decays of ^{22}Na , $^{26}\text{Al}_g$, ^{13}N , ^{14}C , and ^{59}Ni from the Karlsruhe Chart of Nuclides;
4. (α, γ) from NACRE on ^{12}C , ^{15}N , and ^{18}O , and on ^{14}C from Gai et al. (1987), Hashimoto et al. (1986), and Funck & Langanke (1989);¹
5. (α, n) from NACRE on ^{13}C and ^{22}Ne ;
6. (n, γ) from the compilation by Lugaro (2001, Appendix B), which is largely based on Bao et al. (2000), on ^{12}C , ^{14}N , ^{16}O , ^{21}Ne , ^{20}Ne , ^{22}Ne , ^{23}Na , ^{24}Mg , ^{25}Mg , ^{26}Mg , ^{27}Al , ^{28}Si , ^{29}Si , ^{30}Si , ^{31}P , ^{56}Fe , ^{57}Fe , ^{58}Fe , ^{59}Co , ^{58}Ni , ^{59}Ni , ^{60}Ni , ^{61}Ni , and ^{62}Ni ;
7. (n, p) neutron recycling reactions on ^{14}N (Gledenov et al. 1995) and ^{59}Ni from the Reaclib Data Tables of nuclear reaction rates (1991),² updated version of the compilation by Thielemann, Arnould, & Truran (1986);
8. Light and a heavy neutron sinks account for neutron-absorbing species between ^{32}S and ^{56}Fe and above ^{62}Ni , respectively (see § 4 for details).

We consider the light n -capture reactions that are important to determine the n -density. The efficiency of isotopes to absorb neutrons can be measured by the product of the n -capture, Maxwellian-averaged cross section and the number density of the isotope. Assuming a solar abundance distribution, the 12 most important light n -absorbing isotopes are [in the order of decreasing absorbing efficiency; (n, γ) reaction unless noted]: $^{14}\text{N}(n, p)$, ^{30}Si , ^{27}Al , ^{28}Si , ^{29}Si , ^{25}Mg , ^{16}O , ^{14}N , ^{24}Mg , ^{23}Na , ^{20}Ne , and ^{12}C . The order of this list of n -capture isotopes changes at locations in stars where a nonsolar abundance distribution has been established; e.g., in the ^{14}N pocket (see § 5) the ^{14}N abundance is so high that the n -captures by $^{14}\text{N}(n, \gamma)$ reactions outnumber all other (n, γ) reactions on light elements and are themselves dwarfed by those of $^{14}\text{N}(n, p)^{14}\text{C}$. The long-lived ground state of the unstable nucleus ^{26}Al is also a major neutron poison because of its very large cross sections for (n, p) and (n, α) reactions (Skelton, Kavanagh, & Sargood 1987; Koehler et al. 1997). This nucleus is produced by proton captures on ^{25}Mg during H burning. However, it is efficiently destroyed by neutron captures in the TP convective regions; hence, it is not present in the ^{13}C pocket, and we have omitted it in the computation.

The neutron recycling induced by the $^{14}\text{N}(n, p)^{14}\text{C}$ reaction is of particular importance for the s -process in rotating AGB stars. This reaction deprives the Fe seed and transition elements of available neutrons. The major effect is that the neutron exposure is smaller if ^{14}N is present (see the Appendix). In addition, the $^{14}\text{N}(n, p)^{14}\text{C}$ reaction opens a channel to make the isotope ^{15}N , and hence potentially ^{19}F . ^{14}C has a half-life of 5730 yr. Under the typical conditions

¹ We have used the electronic NETGEN database to retrieve these and other rates (Jorissen & Goriely 2001).

² See <http://ie.lbl.gov/astro/friedel.html>.

of n -production in the interpulse phase ($T = 9 \times 10^7$ K, $\rho = 3700$ g cm $^{-3}$), ^{14}C can capture an α -particle or a proton. The $^{14}\text{C}(\alpha, \gamma)^{18}\text{O}$ reaction is 2.5 times slower than that of $^{13}\text{C}(\alpha, n)^{16}\text{O}$, but still affected by large uncertainties. The p -capture reaction of ^{14}C [$^{14}\text{C}(p, \gamma)^{15}\text{N}$] is 3.7 times faster than that of $^{12}\text{C}(p, \gamma)^{13}\text{N}$ and about as fast as that of $^{13}\text{C}(p, \gamma)^{14}\text{N}$. No other p - or α -capture reactions of ^{14}C are important, and $^{14}\text{C}(n, \gamma)^{15}\text{C}$ can also be neglected.

4. APPROXIMATING THE s -PROCESS WITH A NEUTRON SINK

We introduce two reactions and two artificial particles that together give an estimate of the overproduction of s -process elements and the s -process distribution. First, we consider the reaction $^{62}\text{Ni}(n, \gamma)^{63}\text{G}$, where ^{63}G is an artificial particle with mass number 63. We identify the number abundance of ^{63}G with the combined number abundance of all isotopes heavier than ^{62}Ni :

$$Y(^{63}\text{G}) = \sum_{A=63}^{209} Y(^A\text{S}), \quad (4)$$

where S stands for the element symbol of the respective species with $A > 62$. For a solar composition, the number abundance of ^{63}G is $Y_{\odot}(^{63}\text{G}) = 5.4 \times 10^{-8}$. Starting on ^{56}Fe , a suitable neutron exposure will quickly lead to the formation of heavy particles ^AS (with $A > 62$); hence, the abundance of ^{63}G increases. In order to count the number of neutron captures that occur on species with $A > 62$, we introduce a second reaction and a second artificial particle L, $^{63}\text{G}(n, ^1\text{L})^{63}\text{G}$, which plays the role of heavy neutron sink. The Maxwellian-averaged cross section of ^{63}G is computed in the usual way (Jorissen & Arnould 1989):

$$\sigma(^{63}\text{G}) = Y(^{63}\text{G})^{-1} \sum_{A=63}^{209} \sigma_A Y(^A\text{S}). \quad (5)$$

Neutron captures will occur repeatedly on individual ^{63}G particles, thereby simulating the production of increasingly heavy s -process isotopes. These neutron captures are responsible for the final s -process element distribution of the species represented by ^{63}G . They do, however, not change the number abundance of ^{63}G . The ratio $(\text{L}/\text{G}) = Y(^1\text{L})/Y(^{63}\text{G})$ is similar to the customary quantity n_{cap} (Clayton 1968) and is a measure of the s -process distribution (Fig. 3). In fact, if one defines the artificial sink particle G to be the product of an n -capture on ^{56}Fe , then $(\text{L}/\text{G}) = n_{\text{cap}}$. With our choice of G being the product of a n -capture on ^{62}Ni , n_{cap} is slightly larger than (L/G) for a given neutron exposure because n_{cap} takes into account the n -captures on isotopes from ^{56}Fe to ^{62}Ni . These n -captures mainly take place during the initial phase of the neutron exposure phase for $\tau < 0.1$ mbarn $^{-1}$.

The neutron cross section of the sink particle ^{63}G depends on the abundance distribution of the particles it represents. In Figure 4 the Maxwellian-averaged sink cross section at 8 keV according to equation (5) is shown during calculations of the s -process nucleosynthesis with the network including neutron captures on all isotopes up to Pb, starting with a solar abundance distribution of trans-iron elements. The variation of $\sigma(^{63}\text{G})$ reflects the changing abundance distribution of heavy elements. Initially, species accumulate at

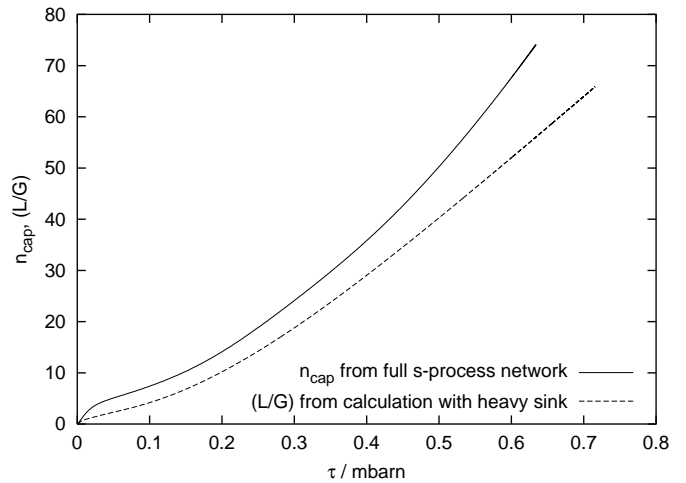


Fig. 3.—Comparison of the s -process parameters n_{cap} and L/G as functions of τ . The quantity n_{cap} is computed with a full s -process network calculation, while the ratio L/G comes from the calculation in which the s -process is approximated with a sink. The first increase of n_{cap} with respect to L/G at very low τ is due to neutron captures on isotopes from ^{56}Fe to ^{62}Ni . From $\tau \sim 0.5$ mbarn $^{-1}$ the results obtained with the neutron sink show larger and larger differences than the results obtained with the full s -process network. The neutron sink representation is a valid approximation for $\tau < 0.6$ mbarn $^{-1}$, i.e., in the range of interest for solar metallicity stars.

the stable neutron magic nuclei on the s -process path (^{88}Sr , ^{138}Ba , ^{208}Pb), and the averaged cross section decreases. As more neutrons are released, the contribution of species in between increases and finally dominates the sink cross section. The choice of a constant sink neutron cross section for the entire s -process simulation is the largest individual uncertainty when approximating the s -process with artificial

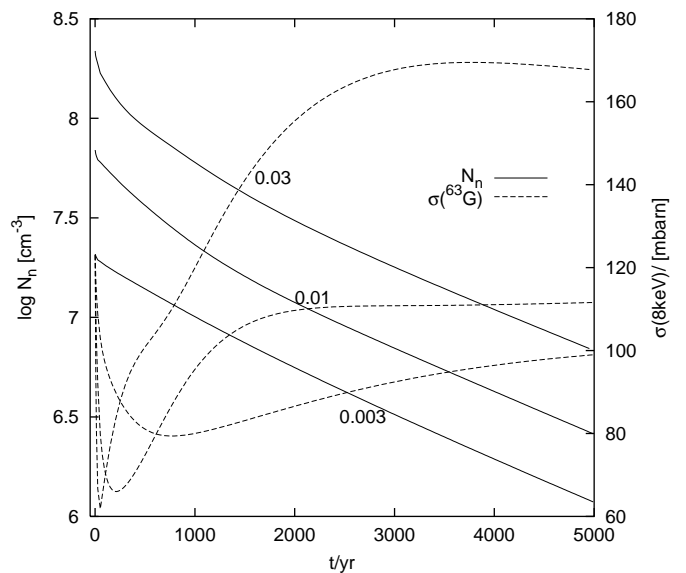


Fig. 4.—Neutron density (solid lines, left ordinate) and Maxwellian-averaged neutron capture cross section (dashed lines, right ordinate) of sink particle ^{63}G (described in § 4) as a function of time from s -process calculations as those performed for Fig. 2 with a network including all heavy elements up to Pb. Three test calculations are presented, starting with three different amounts of ^{13}C mass fractions (indicated by the labels). The variation of the cross section of ^{63}G reflects its dependence on the abundance distribution of the species represented by the sink particle.

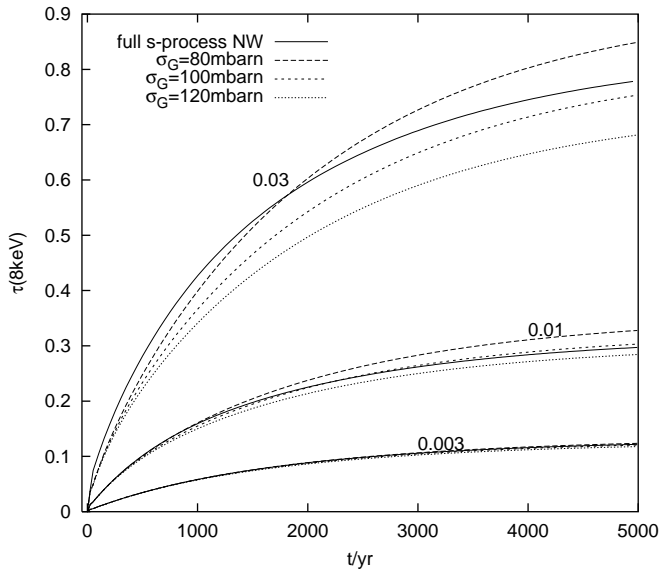


FIG. 5.—Evolution in time of the neutron exposure τ for the three calculations shown in Fig. 4, represented by the solid lines (initial ^{13}C mass fractions indicated by the labels). Each calculation is compared to three tests computed with different values of the Maxwellian-averaged neutron capture cross section of the neutron sink reaction $\sigma(^{63}\text{G})$ described in § 4.

sink reactions, as described above. However, it turns out that the error introduced by using a constant sink cross section is sufficiently small for our purpose. In Figure 5 we show the neutron exposure of calculations with the sink treatment with three choices of the sink cross section as compared with s -process calculations performed with a network including neutron captures on all isotopes up to Pb for the three cases of Figure 4. For low neutron exposures, the influence of the sink cross section is small, because the neutron density is dominated by ^{56}Fe and the lighter neutron capture elements. For the s -process in the partial mixing zone of stars of solar metallicity, the most important range for τ is between ~ 0.2 and 0.5 mbarn^{-1} . We choose for our simulations $\sigma(^{63}\text{G}) = 120 \text{ mbarn}$, which reproduces the neutron exposure from the s -process calculation up to Pb within 10%.

We also introduced a light neutron sink reaction to take into account neutron captures on elements from S to Mn, which are missing in our network. For this reaction, which plays only a minor role, we have used the value $\sigma_{\text{light}}(8 \text{ keV}) = 7.36 \text{ mbarn}$ given by Lugaro (2001).

5. MIXING FROM HYDRODYNAMIC OVERSHOOT

The hydrodynamical properties of convection inevitably result in some turbulent mixing into the stable layers adjacent to convectively unstable regions. In fact, any model of convection in the hydrodynamical framework predicts that the turbulent velocity field decays roughly exponentially inside the stable layers (see, e.g., Xiong 1985; Freytag, Ludwig, & Steffan 1996; Asida & Arnett 2000). A depth- and time-dependent hydrodynamic overshoot approximation has been used in a number of recent studies (Herwig et al. 1997; Mowlavi 1999; Mazzitelli, D’Antona, & Ventura 1999; Salasnich, Bressan, & Chiosi 1999; Herwig 2000; Cristallo et al. 2001), with the aim to capture the main

consequences of hydrodynamic mixing into the stable layers induced by convection.

5.1. Third Dredge-up and $\text{H}/^{12}\text{C}$ Partial Mixing Zone

It has been shown by Herwig (2000) that overshoot at all convective boundaries, including the base of the convective envelope and the bottom of the He flash convection zone, strongly increases the efficiency of the third dredge-up at low core masses. This is required observationally in order to reproduce the observed C star luminosity function in the Magellanic Clouds (Richer 1981; Frogel et al. 1990). Synthetic models of the AGB phase in which the third dredge-up parameter is derived observationally have demonstrated that typically efficient third dredge-up must take place at core masses as low as $0.58 M_{\odot}$ (Marigo et al. 1996), or at even lower core masses around $0.54 M_{\odot}$ according to a more recent analyzes by Marigo et al. (1999). This condition is not met by most stellar models, including those of Mowlavi (1999), who considers hydrodynamic overshoot only at the bottom of the convective envelope (see his Fig. 10b for a comparison of third dredge-up efficiencies found by different authors). The model grid of Herwig, Blöcker, & Driebe (2000), which includes overshoot at all convective boundaries, includes cases (e.g., the $2 M_{\odot}$, $Z = 0.01$ case) that cover the low C star luminosity tail, as required by observations. The third dredge-up properties of AGB models are important for the s -process because third dredge-up is needed to bring the processed material to the surface. Hydrodynamic overshoot creates a partial mixing zone at the core-envelope interface with a continuous decrease of the $\text{H}/^{12}\text{C}$ ratio from the envelope into the intershell layers (Herwig et al. 1997; Herwig 2000).

The global properties of the s -process can be reproduced with a partial mixing zone resulting from hydrodynamic overshoot (Goriely & Mowlavi 2000; Lugaro & Herwig 2001). The main features of the s -process overabundance distribution are mainly determined by the regions of the pocket that have the largest neutron exposures, and not so much by the detailed shape of the $\text{H}/^{12}\text{C}$ profile within the partial mixing zone. Even if the treatment of hydrodynamic overshoot according to an exponentially decaying velocity field is not correct and the actual functional dependence of overshoot efficiency with depth is somewhat different, the s -process will most likely be affected only slightly as long as the $\text{H}/^{12}\text{C}$ profile is somehow continuous. For example, Denissenkov & Tout (2003) investigate gravity waves below the convective envelope as a cause for extra mixing to produce partial mixing of protons and ^{12}C . This mixing process is another way of looking at the mixing resulting from the perturbation of the convective boundary due to turbulence and leads to neutron exposures in the region close to that of previous models featuring a continuous decrease of the proton abundances into the ^{12}C -rich core.

An additional effect is introduced in models that consider overshoot at all convective boundaries (Herwig 2000). In these models the ^{12}C abundance in the intershell is about twice as large as that in models without overshoot at the base of the He-shell flash convection zone. Lugaro et al. (2003b) have shown that the neutron exposure in the s -process layer is proportional to the ^{12}C abundance in the intershell. Hence, in models that consider overshoot at the base of the He-shell flash convection zone, the neutron

exposure in the s -process layer is higher than in models that do not include this overshoot.

5.2. How Much Overshoot?

The initial computations of AGB stars with hydrodynamic overshoot were carried out with an exponential overshoot parameter of $f = 0.016$, which was motivated by the efficiency derived from convective core overshoot of main-sequence stars. The effective mass of the partial mixing zone where the neutrons are efficiently released is confined within the region where the proton abundance follows $-2 < \log X_p < -3$ (for an intershell ^{12}C mass fraction of $\sim 20\%$; Goriely & Mowlavi 2000). According to this criterion the mass of the s -process layer computed with $f = 0.016$ is only $\sim 10^{-6} M_\odot$, which is much smaller than required (see § 2).

However, one overshoot efficiency parameter will not apply to all convective boundaries during all evolutionary phases. After Shaviv & Salpeter (1973) first considered the possibility of the convective overshoot, several studies have used a very simple prescription in which convective mixing was treated instantaneously and overshoot was simply a matter of extending the instantaneously mixed region by some fraction of the pressure scale height. In this approximation main-sequence core overshoot should extend by about $0.2H_p$ (see, e.g., Schaller et al. 1992 and references therein). Alongi et al. (1991) argued that overshoot of $0.7H_p$ below the envelope of red giant stars could align the location of luminosity bump with observations. The two-dimensional radiation hydrodynamic simulations by Freytag et al. (1996) have shown that the shallow surface convection zone of white dwarfs has exponential overshoot mixing according to an overshoot parameter of $f = 1.0$, while the convection zone simulation of A stars shows $f = 0.25$. For the oxygen-burning layer in presupernova models, Asida & Arnett (2000) found perturbations of the stable layers reaching $1H_p$ beyond the formal convective boundary. Thus, there is ample indication that the overshoot efficiency is not the same at different convective boundaries. However, convective overshoot is not a stochastic process as long as the convective turnover timescale is shorter than the thermal timescale of the region that hosts the convective boundary. For similar convective boundaries one should expect a similar overshoot efficiency. This expectation is supported by two-dimensional hydrodynamical computations by Deupree (2000), who showed that the core overshoot distance of ZAMS stars varies only mildly with stellar mass.

Here we choose an exponential overshoot parameter for the hydrodynamic overshoot at the bottom of convective envelope of $f = 0.16$. This larger overshoot is only applied during the third dredge-up phase. This has no major effect on the properties of the models, other than stretching the partial mixing zone and, consequently, the ^{13}C and ^{14}N profiles in that layer over a larger mass range. The peak neutron exposure and the s -process abundance distribution in the partial mixing layer are not much changed. As a side effect the third dredge-up efficiency is slightly increased, by $\sim 20\%$.

As mentioned in § 1, observations as well as the analysis of presolar meteoritic SiC grains suggest that stars with otherwise identical initial conditions have a range of s -process efficiencies. Such a range cannot be expected to result from overshoot since such a mechanism is not expected to be a stochastic process.

5.3. Neutron Production for the s -Process in the Overshoot Model

We model the abundance evolution in the partial mixing zone during the seventh interpulse phase of the $3 M_\odot$, $Z = 0.02$ sequence of Herwig et al. (2000), with an overshoot efficiency $f = 0.16$ during the third dredge-up phase. We use the postprocessing code (SBM6) described in § 3 because the computation of the stellar evolution does not include all the species and reactions needed to study the s -process. As initial conditions we use the thermodynamic and abundance profiles from the stellar evolution model at the end of the third dredge-up phase after the TP. These profiles are mapped to the equidistant, Lagrangian postprocessing grid and then evolved according to the stellar structure models at a series of times throughout the interpulse phase.

We start the simulation with the partially mixed $\text{H}/^{12}\text{C}$ zone of $\sim 10^{-4} M_\odot$ that has formed at the end of the third dredge-up phase as a result of time- and depth-dependent hydrodynamic overshoot (top panel, Fig. 6). In this model no mixing takes place during the interpulse phase. In the middle panel of Figure 6 the ^{13}C neutron source has started releasing neutrons, and up to 10% of the ^{13}C abundance has been consumed. In the upper part of the partial mixing zone, where ^{14}N dominates, the majority of neutrons are absorbed by the $^{14}\text{N}(n, p)^{14}\text{C}$ reaction. This can be seen from the profile of ^{14}C . The maximum neutron density is $5.7 \times 10^6 \text{ cm}^{-3}$

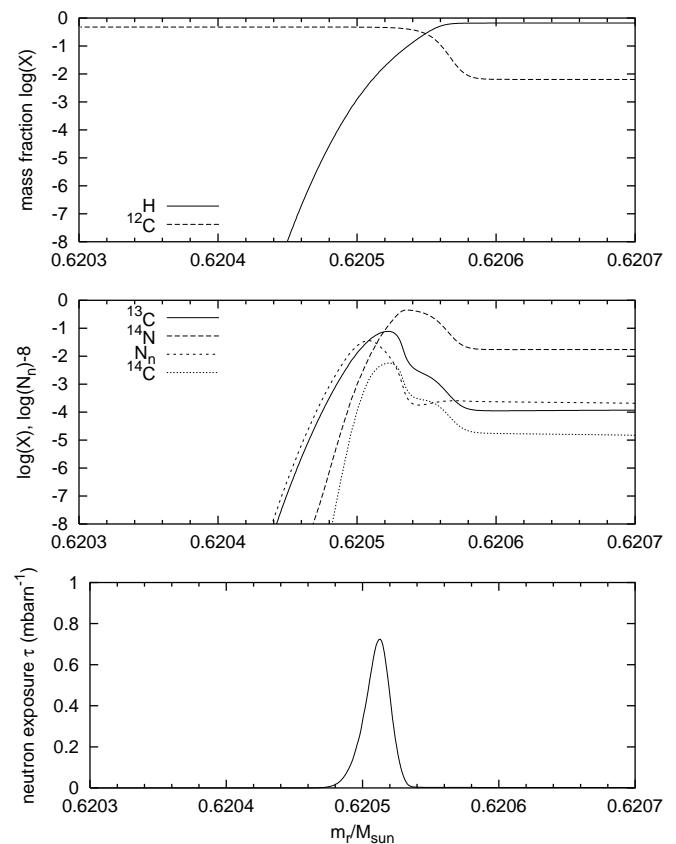


FIG. 6.—Abundance profiles in the partial mixing zone at three times during the seventh interpulse phase of the model with hydrodynamic overshoot and no rotation. *Top*: First postprocessing model after the end of the third dredge-up phase. *Middle*: 10% of ^{13}C is burned by $^{13}\text{C}(\alpha, n)^{16}\text{O}$. *Bottom*: Neutron exposure τ at end of the s -process in the partial mixing zone when the ^{13}C neutron source is exhausted.

at that time, and it subsequently reaches a peak value of $1.1 \times 10^7 \text{ cm}^{-3}$. The bottom panel of Figure 6 shows the total neutron exposure in the s -process layer before it is engulfed by the subsequent He flash convection zone. A maximum neutron exposure $\tau = 0.72 \text{ mbarn}^{-1}$ is found. This is about a factor of 2 larger than in previous s -process simulations of the partial mixing scenario (Goriely & Mowlavi 2000) because in our overshoot models the ^{12}C intershell abundance is larger than in models that do not use overshoot at the bottom of the He flash convection zone.

In comparison to the observational constraints for the partial mixing and s -process layer derived in § 2, we find that the neutron exposure in this model with hydrodynamic overshoot at all convective boundaries is too large. Lugaro et al. (2003b) concluded that to match observed stellar s -process abundance patterns, the overshoot at the bottom of the He flash convection zone should be smaller than that used by Herwig (2000), $f = 0.016$. For example, the higher temperatures in the He flash convection zone due to overshoot result in very large $^{96}\text{Zr}/^{94}\text{Zr}$ ratios, in contradiction with measurements in mainstream presolar meteoritic SiC grains. The temperature in the He flash convection zone decreases with the stellar mass. However, some SiC grains show almost no presence of ^{96}Zr , and they are difficult to explain by current models, even by considering stars with mass as low as $1.5 M_{\odot}$ (Lugaro et al. 2003a) and no overshoot included. The inclusion of overshoot at the base of the He flash convection zone increases the temperature for a given stellar mass, making it even more difficult to explain these data. On the other hand, current models of hydrogen-deficient post-AGB stars (Herwig et al. 1999) can only reproduce the abundance patterns observed in PG 1159-type objects and central stars of planetary nebulae of spectral type [WC] (Koesterke & Hamann 1997; Dreizler et al. 1996) with AGB progenitor models including intershell overshoot. Further investigations of extra mixing have to address whether the constraints from s -process branchings and from subsequent evolutionary stages can be resolved in well-adjusted models. The mass of the layer in which significant overproduction factors of s -process elements can be expected is in our calculation of the order of $\sim 3 \times 10^{-5} M_{\odot}$, about a factor of 2 less than the minimum pocket mass required according to the estimates in § 2. The choice of the overshoot parameter at the base of the convective envelope only affects the extent in mass of the partial mixing zone and affects very little the s -process distribution. The latter is determined by the neutron exposure in the pocket. For that reason one cannot remove the problem of the large neutron exposure in our overshoot model by a fine-tuning of the overshoot parameter at the base of the convective envelope.

This can easily be shown with a numerical test carried out with a parametric s -process code, such as that used by Lugaro et al. (2003b and references therein). We made four runs of the s -process model with radiative ^{13}C burning through 13 TP events and mixing episodes according to the stellar evolution model including overshoot, as described in Lugaro et al. (2003b). To select the effect of varying of the ^{13}C pocket mass only, we neglect the contribution of the ^{22}Ne neutron source during the He-shell flash. The benchmark (BM) case corresponds to the ^{13}C pocket obtained with an exponential overshoot parameter of $f = 0.128$ at the bottom of the convective envelope. The pocket is computed starting from an intershell ^{12}C mass fraction of 0.43 and is kept identical in all the interpulse phases. We multi-

ply/divide the mass of the pocket as indicated in Table 1, which approximates the effect of larger/smaller f -values. Note that this is different than changing the ^{13}C abundance in the pocket, as is done in order to obtain a spread in neutron exposures by Busso et al. (2001). Table 1 gives s -process indices at the stellar surface at the end of an AGB model sequence. In all cases $[\text{hs}/\text{ls}] > 0$, clearly in contrast to the observed negative $[\text{hs}/\text{ls}]$. The smallest $[\text{hs}/\text{ls}]$ values that are closest to the observed values correspond to almost no s -process overproduction ($[\text{ls}/\text{Fe}]$ and $[\text{hs}/\text{Fe}] \sim 0$) and must be excluded.

6. MIXING IN ROTATING AGB STARS

For the formation of the ^{13}C pocket and the s -process in TP-AGB stars, the most relevant rotationally induced mixing instability is caused by shear at locations of large angular velocity gradients. In order to anticipate rotationally induced mixing events, it is therefore important to consider the angular velocity evolution throughout the TP cycle. Throughout this and the following section we make use of the interpulse phase $\phi = (t - t_0)/\Delta t$, where t_0 is the time of the TP, i.e., the peak He-burning luminosity, and Δt is the interpulse period of $3 \times 10^4 \text{ yr}$.

The evolution of angular velocity in the intershell region during the 25th interpulse period of our $3 M_{\odot}$ rotating TP-AGB model star is shown in Figure 7. The main features of the angular velocity evolution can be understood by redistribution of angular momentum in the convective regions and conservation of angular momentum in contracting or expanding stable layers. The first profile at $\phi = -0.0536$ shows a model of stable H burning during the interpulse phase shortly before the He-shell flash. The H shell is located just below the mass coordinate $0.746 M_{\odot}$. The steep jump at $\sim 0.741 M_{\odot}$ marks the largest extent of the He flash convection zone during the previous TP. The He flash convection zone redistributes angular momentum from the faster rotating C/O core throughout the intershell and the layers just below the H-rich envelope. The profile shows a

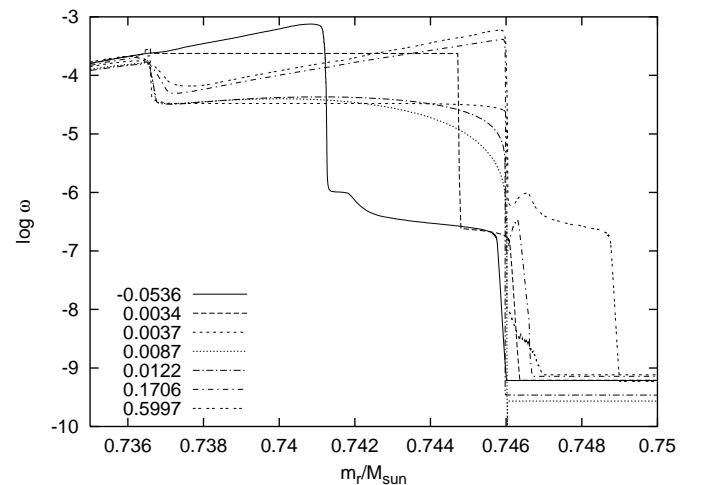


Fig. 7.—Evolution of angular velocity profiles through the 25th interpulse-pulse cycle. Labels give interpulse phase $\phi = (t - t_0)/\Delta t$, where the previous pulse, i.e., the maximum He-burning luminosity, has occurred at t_0 ; the interpulse period is $\Delta t = 3 \times 10^4 \text{ yr}$. The mass range covers the intershell region from the top of the C/O core (location of the He shell) to the bottom of the convective envelope.

plateau between 0.741 and $0.746 M_{\odot}$. This region contains the H-shell ashes that have been deposited there by the outward-burning H shell. The angular velocity is larger in this area than in the convective envelope above the H-burning shell. Angular momentum is efficiently distributed by convection throughout the convective envelope, which rotates almost rigidly. However, the H-burning ashes contract onto the core, and therefore the angular velocity increases; hence, the plateau between 0.741 and $0.746 M_{\odot}$ is formed.

At $\phi = 0.0034$ the He flash convection zone has formed, and the mass layers covered by convection are spun up. At this time the He flash convection zone reaches up to mass coordinate $0.745 M_{\odot}$. Between this and the following profile at $\phi = 0.0037$ the He flash convection zone reaches its fullest extent up to $0.746 M_{\odot}$ (just below the location of the H-burning shell before the TP). In addition, the intershell region is expanding because of the energy provided by the He flash. This leads to a reduction of the angular velocity in the intershell. This effect is still present at $\phi = 0.0087$, until contraction resumes and the angular velocity in the intershell region increases accordingly (profiles $\phi = 0.0122$ – 0.1706). The angular velocity profiles at later times show again the formation of a plateau between 0.746 and $0.749 M_{\odot}$, where the H shell is now located, because of deposition of H-shell ashes on top of the core.

From the evolution of the angular velocity in rotating TP-AGB stars we can anticipate the following mixing properties. Efficient shear mixing will take place at $\sim 0.746 M_{\odot}$ after the formation of the large angular velocity gradient. This gradient forms because two convective regions extend to these mass coordinates from below and above in short succession. The He flash convection first taps the reservoir of high angular momentum in the core. Then the convective envelope establishes contact between the fast-rotating intershell and the slow-rotating envelope. At this interface rotationally induced shear mixing will be most efficient in acting on abundance gradients. The timescale to establish a partial mixing zone of hydrogen and ^{12}C as needed for the formation of the ^{13}C pocket is limited to the time interval when the envelope and the intershell are in contact, i.e., between the end of the third dredge-up and the reignition of the H-shell. This period lasts 2000–3000 yr (Fig. 1). However, as can be seen in Figure 7, the steep angular velocity gradient remains at this mass coordinate after the formation of the partial mixing zone, and shear mixing at this location will persist throughout the intershell period.

Correspondingly, two mixing periods during the interpulse phase resulting from rotation can be distinguished, as shown by the temporal evolution of the mixing coefficient presented in Figure 8. During the initial envelope-core contact period at the end of the third dredge-up, a partial mixing zone of protons and ^{12}C forms (top panel, Fig. 9). The mixing efficiency in Eulerian coordinates at this time is $\log D_r \sim 5$ (in cgs units), but decreasing rapidly at a timescale of ~ 1000 yr. However, after the TP the mass gradient in the partial mixing zone increases steadily as the intershell layers contract and evolve toward a preflash structure. For assessing the effect on the abundance evolution, the Lagrangian mixing coefficient should be considered:

$$D_m = \left(\frac{dm}{dr}\right)^2 D_r = (4\pi\rho r^2)^2 D_r, \quad (6)$$

where all symbols have their usual meaning.

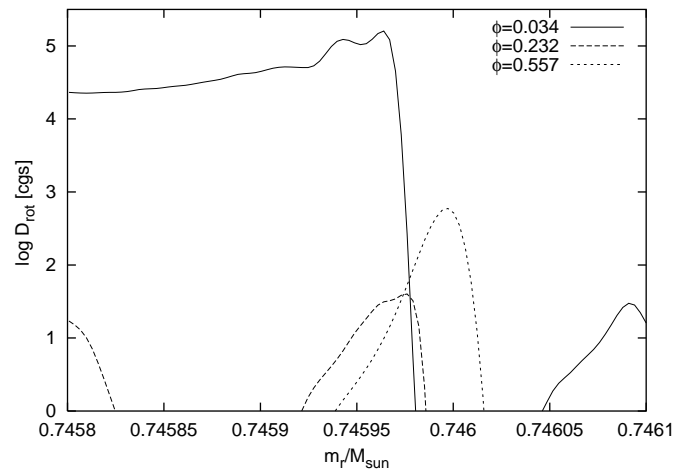


FIG. 8.—Evolution of mixing coefficient due to rotationally induced mixing during the interpulse phase; labels give interpulse phase $\phi = (t - t_0)/\Delta t$, where the previous pulse, i.e., the maximum He-burning luminosity, has occurred at t_0 ; the interpulse period is $\Delta t = 3 \times 10^4$ yr. Two different mixing periods resulting from rotation occur in the partial mixing zone during the interpulse period (see text).

In Table 2 we give the mixing properties in the partial mixing zone at three different times: an early phase soon after the pulse, a phase just before the release of neutrons starts, and a phase after the neutron source ^{13}C is exhausted.

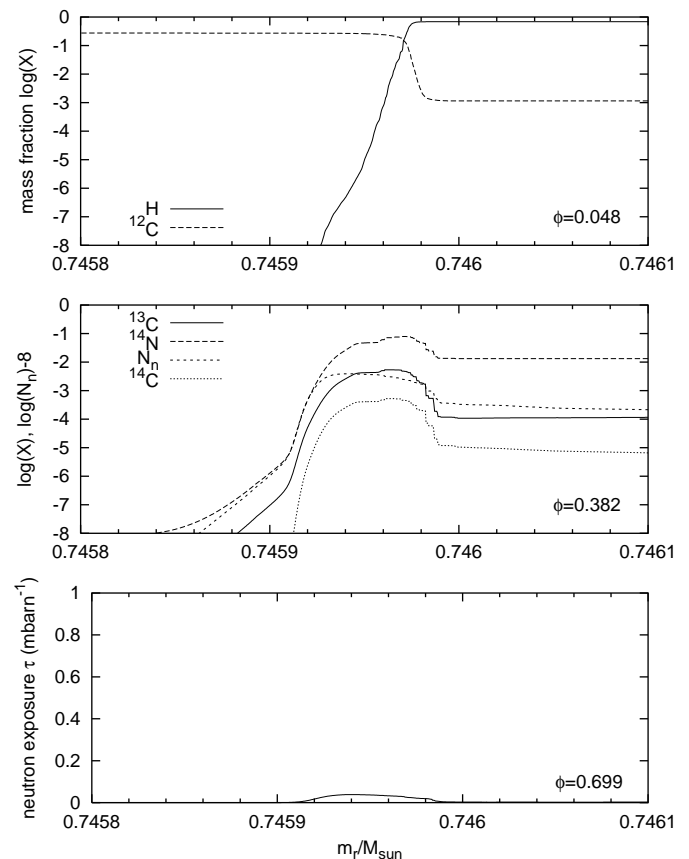


FIG. 9.—Same as Fig. 6 for the simulation at the 25th interpulse phase including rotation and no hydrodynamic overshoot. The middle panel shows the same interpulse phase as the middle panel in Fig. 6 with respect to the nuclear lifetime of ^{13}C against α -capture.

TABLE 2

MIXING COEFFICIENTS AND LAGRANGIAN MIXING EFFICIENCY IN THE PARTIAL MIXING LAYER OF THE AGB MODEL INCLUDING ROTATION

ϕ	dm/dr^a ($M_\odot \text{ cm}^{-1}$)	$\log D_r^b$ ($\text{cm}^2 \text{ s}^{-1}$)	$\log D_m$ ($M_\odot^2 \text{ yr}^{-1}$)	Δt_{mix} (yr)	Δm_{mix} (M_\odot)
0.034	5.4×10^{-14}	~ 5.0	-14.0	1440 ^c	3.7×10^{-6}
0.232	9.2×10^{-12}	~ 1.5	-13.1	8560 ^c	2.7×10^{-5}
0.557	3.6×10^{-11}	~ 2.8	-10.6	2900 ^d	2.7×10^{-4}

^a At $m_r = 0.745965 M_\odot$.

^b Maximum; see Fig. 8 for the overall distribution in mass.

^c Time since TP.

^d Nuclear lifetime of ^{13}C against α -capture $\tau_\alpha(^{13}\text{C})$.

Despite the comparatively large mixing coefficients, rotationally induced mixing is not important immediately after the initial formation of the partial mixing zone. By the time the neutron source is about to be activated the mass gradient has increased by more than 2 orders of magnitude, which more than offsets the decrease of the geometrical mixing coefficient. The Lagrangian mixing range then exceeds the mass of the initial partial mixing zone. This trend continues throughout the time of occurrence of the s -process during the interpulse phase, as the intershell layer and the partial mixing zone gradually contract.

Finally, we note that the present model with rotation does not show sufficient third dredge-up. This has already been reported by Langer et al. (1999) and is evident from their Figures 3 and 4. We found that the third dredge-up in models of rotating AGB stars is related to the efficiency of μ -gradients to inhibit mixing. This is a somewhat uncertain parameterized property of rotating stellar models, and a different approach in describing this effect could change the resulting third dredge-up.

6.1. Neutron Production for the s -Process with Rotation

We model the abundance evolution in the partial mixing zone during the 25th interpulse phase of a stellar model of $3 M_\odot$, $Z = 0.02$ and an initial equatorial rotation velocity of 250 km s^{-1} (Langer et al. 1999). The core mass at this interpulse phase is $M_c = 0.746 M_\odot$, and the third dredge-up only just dips into the C-rich intershell. To compute the s -process, we used the postprocessing code (SBM6) described in § 3. As in the computation with overshoot, we use as initial conditions the thermodynamic and abundance profiles from the stellar evolution model at the end of the third dredge-up. We map these profiles to the equidistant, Lagrangian postprocessing grid and then evolve them according to the stellar structure models at a series of times throughout the interpulse phase. As a result of shear mixing due to the large angular velocity gradient immediately after the end of the third dredge-up, a partial mixing zone forms (top panel, Fig. 9) similar to that in models with diffusive overshoot (Fig. 6). The partial mixing zone defined as having a proton abundance of $-2 < \log X(p) < -3$ has a mass of $M_{\text{PM}} = 6 \times 10^{-6} M_\odot$.

As described above, throughout the interpulse period shear mixing at the former core-envelope interface continues at a low level. This has two effects on the ^{13}C initially formed in the partial mixing zone. First, the ^{13}C is spread out, and hence diluted, over the mass range subject to shear mixing. Second, the ^{14}N and the ^{13}C pockets, which are well separated in the overshoot model, are effectively mixed. As

a result the ^{14}N abundance exceeds the ^{13}C abundance everywhere in the pocket (middle panel, Fig. 9). In this situation most neutrons released by $^{13}\text{C}(\alpha, n)$ are absorbed by the reaction $^{14}\text{N}(n, p)^{14}\text{C}$ rather than by heavy nuclei. Because of the increased amount of neutron absorbers, the neutron density is drastically reduced; the maximum neutron density is $N_n = 2.6 \times 10^6 \text{ cm}^{-3}$. This corresponds to the very small neutron exposure obtained in this model (bottom panel, Fig. 9). The activation of the $^{14}\text{N}(n, p)^{14}\text{C}$ reaction can be seen from the ^{14}C profile in the middle panel. Protons released by this reaction are captured by ^{12}C , building more ^{13}C , as well as by ^{13}C itself (and by ^{18}O ; see discussion in § 8).

In comparison to the basic requirements for the s -process layer derived in § 2, we conclude that this particular model of rotational mixing in the TP-AGB interpulse period cannot produce the s -process abundance patterns observed in stars of solar metallicity. The neutron exposure reaches only $\tau = 0.04 \text{ mbarn}^{-1}$, too small for any significant s -process enhancement. As far as the mass of the s -process layer is concerned, we note that shear mixing has caused a substantial broadening. In the end, a zone of $5 \times 10^{-5} M_\odot$ has experienced a low neutron irradiation.

One peculiarity of s -process simulations including mixing throughout the interpulse period concerns the sensitivity to uncertainties of the nuclear reaction rates. In the parameterized s -process without mixing during the interpulse, each layer is treated individually, and all ^{13}C is burnt before the onset of the next He-shell flash. As a result, for example, a different $^{13}\text{C}(\alpha, n)^{16}\text{O}$ rate, as long as it allows all ^{13}C to be consumed during the interpulse period, would lead to a slight time shift of the neutron release, but in the end this does not affect the neutron exposure. The case with mixing throughout the interpulse is different because of the more important recycling of neutrons by $^{14}\text{N}(n, p)^{14}\text{C}$ and $^{12}\text{C}(p, \gamma)^{13}\text{N}$. For example, we find that the neutron exposure increases by about 20% when using the NACRE (Angulo et al. 1999) $^{13}\text{C}(\alpha, n)^{16}\text{O}$ rate instead of the Caughlan & Fowler (1988) rate.

In summary, we have demonstrated the main properties of partial mixing layers for the s -process due to rotationally induced mixing and to hydrodynamic overshoot. Neither model seems to be consistent with the observed properties. The overshoot model shows some problems related to the overshoot at the base of the He flash convection. The model including rotational mixing shows that the s -process during the interpulse is easily prevented if the delicate process of ^{13}C formation and neutron release is disturbed by mixing. In fact, our preliminary model of an AGB star evolving from a main-sequence star rotating more slowly than the model presented above indicates that also in this case the s -process nucleosynthesis during the interpulse period is very much inhibited by the rotation induced mixing.

7. SYNTHETIC MIXING MODELS

In the previous section we encountered the limitations of both mixing processes, hydrodynamic overshoot and rotationally induced mixing. Here we want to explore the possibility that some combination of both processes may provide a satisfactory mixing law for the s -process. To that end we construct some synthetic postprocessing models that include overshoot and rotation in a simple parametric scheme.

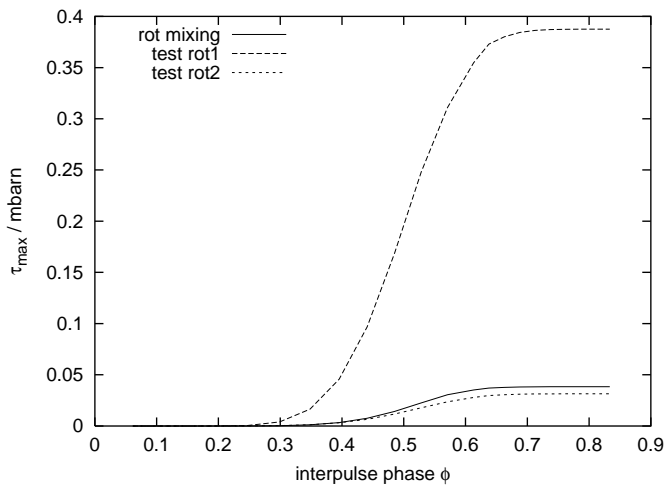


FIG. 10.—Maximum neutron exposure in the stellar layer where the s -process occurs during the TP-AGB interpulse period as a function of phase ϕ . The solid line is the result of detailed computation with rotational mixing (shown in Fig. 9), and the dashed lines show test calculations (see § 7).

We approximate the details of rotationally induced mixing by assuming a constant mixing coefficient D_{IP} throughout the interpulse phase for the postprocessing simulation of the s -process layer. To show that this approach leads to the same results as the detailed computation presented in § 6.1, we compare the evolution of the neutron exposure with time with that obtained in the detailed computation with that obtained in two test cases (Fig. 10). Test rot1 is computed by starting from the partial mixing zone obtained in the rotation sequence (top panel, Fig. 9), but excluding any further mixing during the interpulse. The maximum neutron

exposure is $\tau \approx 0.38 \text{ mbarn}^{-1}$, much higher than in the case in which mixing continues during the interpulse and very similar to that found in other partial mixing models without rotation. However, the neutron exposure integrated over the simulated mass range is 2 times smaller in test case rot1 than in the case in which the further mixing during the interpulse is included. This reflects the higher degree of n -recycling in a region of wider mass in the case in which rotation mixing during the interpulse is included. Test rot2 is computed by starting again from the partial mixing zone obtained in the rotation sequence and applying a constant Eulerian mixing coefficient $\log D_{IP} = 1$ (cgs units) across the simulation range. This procedure can approximately reproduce the key quantities of the detailed postprocessing simulation presented in § 6.1: $M_{MP} \leq 10^{-4} M_{\odot}$ and $\tau_{\max} \sim 0.03 \text{ mbarn}^{-1}$. The fact that the test case rot2 approximates the results of the detailed simulation confirms that a constant mixing coefficient throughout the interpulse period mimics the second phase of rotationally induced mixing that is responsible for the admixture of the ^{14}N neutron poison and the dilution of the ^{13}C pocket.

With this simple representation we study the effect that mixing of the s -process layers during the interpulse might have on the partial mixing zone formed as a result of hydrodynamic overshoot. We perform another set of simulations in which we start with the partial mixing layer produced from hydrodynamic overshoot (shown in the top panel of Fig. 6). A constant mixing coefficient is imposed during the interpulse simulation. Cases for four different interpulse mixing efficiencies are shown in Figure 11. Even with very weak constant mixing of $\log D_{IP} = -2$ the peak neutron exposure is somewhat reduced compared to the overshoot case without interpulse mixing (shown in Fig. 6). For faster interpulse mixing, the s -process layer becomes broader, and the final neutron exposure declines.

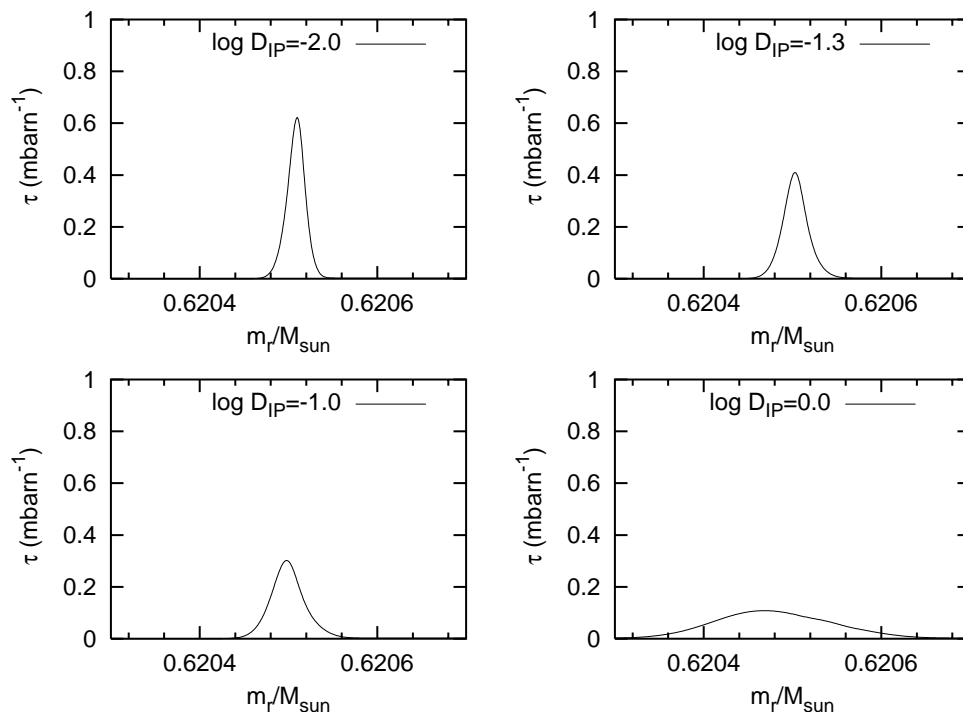


FIG. 11.—Final neutron exposure profiles in the s -process layer of simulations with a synthetic mixing law, combining the initial formation of a partial mixing layer by overshoot with a constant interpulse mixing coefficient that mimics the effect of shear mixing (see text for details).

From these tests we tentatively propose a two-step mixing scheme for the *s*-process in AGB stars. At the end of the third dredge-up a fast-mixing process induced by the convectively unstable envelope leads to the formation of a partial mixing zone. A mass interval of $\approx 5 \times 10^{-5} M_{\odot}$ should have a proton abundance of $-2 < \log X(p) < -3$. The intershell ^{12}C abundance should be larger than in models that confine mixing in the He-shell flash convection zone strictly to within the Schwarzschild boundaries. Because of mixing during the interpulse phase, the neutron release is modulated (in any case, reduced), and a set of otherwise identical stars with a variety of mixing efficiencies at the core-envelope layers will display a spectrum of neutron exposures. In this scenario involving hydrodynamic overshoot as well as interpulse mixing, the efficiencies needed to cover the spread in *s*-process efficiencies observed in stars (Busso et al. 2001) and presolar grains (Lugaro et al. 2003a) can be achieved with mixing efficiencies of the order $\log D_{\text{IP}} \approx 0$ to -1.3 . This range is not currently reproduced by stellar evolutionary sequences including rotation, which predict much larger mixing efficiencies (see § 6.1). Smaller mixing efficiencies would result from a smaller angular velocity gradient at the core-envelope interface and/or a smaller rotation rate. This could be achieved by a more efficient angular momentum transport during the progenitor evolution. Efficient third dredge-up and/or penetration of the convective pulse into the core might affect the mixing properties due to rotation since angular momentum could be transported out of the core into the envelope and carried away by mass loss. This effect is not present in our computation since our models do not show efficient third dredge-up. Moreover, in our models we have not considered magnetic fields that could enhance the coupling of core and envelope and decelerate the core (Spruit 1998).

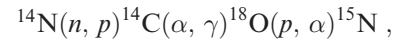
8. FLUORINE PRODUCTION IN MODELS WITH ROTATION

Jorissen, Smith, & Lambert (1992) have observed high enhancements of fluorine in AGB stars. The solar abundance is $X(^{19}\text{F}) = 4.1 \times 10^{-7}$, and observationally, $X(^{19}\text{F}) = 6.6 \times 10^{-7}$ at the start of the AGB phase (average of K and M giants). The typical abundance of ^{19}F in TP-AGB stars (S, M, and C stars) is $X(^{19}\text{F}) \approx (4.5 \pm 4) \times 10^{-6}$. In particular, the N-type carbon stars show a large spread in ^{19}F abundances within a small range of C/O values. Overall, TPs appear to cause a 10-fold increase in ^{19}F as a result of TP and/or interpulse nucleosynthesis and third dredge-up. While the observed correlation of fluorine enhancement with *s*-process enhancement is reproduced by current models (see Fig. 13 of Goriely & Mowlavi 2000), the observed correlation of fluorine with carbon remains unsolved.

Several nucleosynthesis paths have been considered, and the most likely involves an (n, p) reaction (Jorissen et al. 1992). Because the $^{19}\text{F}(\alpha, p)^{22}\text{Ne}$ rate is about 10 times larger than the $^{22}\text{Ne}(\alpha, n)^{25}\text{Mg}$ rate at $T = 3 \times 10^8$ K (Caughlan & Fowler 1988; Angulo et al. 1999), ^{22}Ne can be excluded as the *n*-source for the required (n, p) reactions. Even if fluorine is made during the interpulse period, massive AGB stars can be excluded as ^{19}F producers because they have very hot He flash convective zones, in which $^{19}\text{F}(\alpha, p)^{22}\text{Ne}$ is very efficient. Moreover, in massive AGB stars, proton captures at the hot base of the convective envelope destroy fluorine efficiently.

The $^{13}\text{C}(\alpha, n)$ reaction is activated when the H-burning ashes are engulfed in the convection zone. However, the amount of neutrons released by the ^{13}C from the H-burning ashes is not enough to produce the required abundance of fluorine. Another possible site for the production of fluorine is the nucleosynthesis occurring in the partial mixing zone during the interpulse periods. However, the partial mixing zone is typically unimportant with regard to the production of light elements because its mass is very small. In fact, the inclusion of the partial mixing zone in model calculations does not appear to increase the predicted surface abundance of ^{19}F . This conclusion can be drawn when comparing the abundance of ^{19}F at a given C/O ratio in Figure 12 of Goriely & Mowlavi (2000), who studied fluorine production in AGB stars, including a parametric partial mixing zone, and in Figure 14 of Mowlavi, Jorissen, & Arnould (1996), who did not include a partial mixing zone in their study. Here we check whether rotation can improve the match with observation.

During the interpulse period and in the partial mixing zone, about 80% of the ^{15}N is produced via the chain of reactions



and 20% comes from the reaction $^{14}\text{N}(n, \gamma)^{15}\text{N}$ (Fig. 12). During the interpulse phase the temperature is not high enough for the $^{15}\text{N}(\alpha, \gamma)^{19}\text{F}$ reaction, and the production of fluorine occurs later in the He flash convection zone [note that the $^{15}\text{N}(\alpha, \gamma)^{19}\text{F}$ rate is about 50 times faster than the destruction of ^{19}F by α -capture in the temperature range of interest]. For simplicity we assume that all ^{15}N present in the intershell before the onset of the He flash will be transformed into ^{19}F and that no ^{19}F will be destroyed so that the intershell abundance at the time of the third dredge-up is $X_{\text{IS}}(^{19}\text{F}) \propto M_{^{15}\text{N}}/M_{\text{IS}}$, where $M_{^{15}\text{N}} = X_{\text{PM}}(^{15}\text{N})M_{\text{PM}}$. With equation (1), the observed abundances mentioned above, using $q = 2.3$, $m = 20$, and the other numbers used in § 2, the total ^{15}N production in the partial mixing zone during the interpulse phase must be of the order of $M_{^{15}\text{N}} > 10^{-7} M_{\odot}$ to cover the observational data.

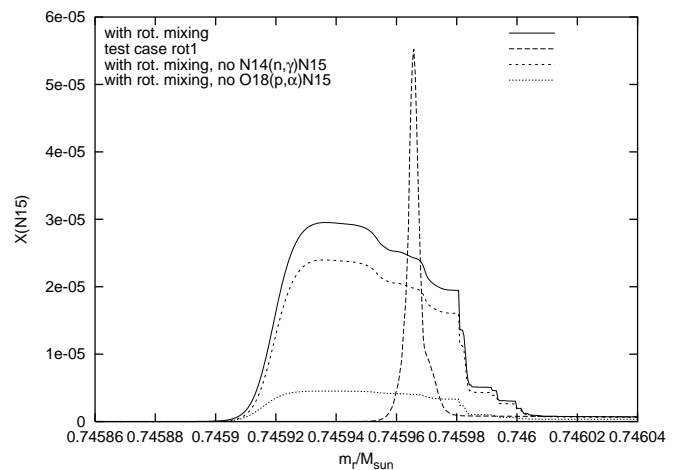


FIG. 12.—Profile of ^{15}N mass fraction across the partial mixing zone at a time close to the maximum neutron density in the simulation with rotation presented in § 6. The long-dashed and dotted lines clarify the contributions by two reaction chains discussed in the text. For comparison the ^{15}N profile for the same time is shown for the test case rot1 presented in § 7.

In Figure 12 we show some results for the ^{15}N production in the partial mixing zone. In the postprocessing model of the sequence including rotation, ^{15}N is produced by the reaction channels described above. The absolute amount is much smaller than needed. However, compared to a case with the same initial partial mixing zone but no interpulse mixing (test case rot1; § 7), the production of ^{15}N is larger by a factor of 2–3. We analyzed the ^{15}N production in the parametric models presented in § 7 that combine an overshooting partial mixing zone with interpulse mixing of the s -process layer. We find that the ^{15}N production increases with interpulse mixing reaching $8 \times 10^{-8} M_{\odot}$ for $D_{\text{IP}} = 0$. If rotation in AGB stars is instrumental in producing ^{19}F , one might expect an anticorrelation of ^{19}F with the s -process index [hs/l_s] as well as with the s -process enhancement. Currently available observational data do not show this. Renewed observational work on ^{19}F in AGB stars is needed, as well as more detailed models. In addition, the question of reaction rate uncertainties has to be revised, in particular in the case of $^{14}\text{C}(\alpha, \gamma)^{18}\text{O}$.

9. DISCUSSION

We have compared two mixing processes for the s -process in low-mass AGB stars. Models that include overshoot at all convective boundaries feature neutron exposures that are larger than allowed to reproduce the observed s -process properties. This is due to the fact that overshoot at the base of the He shell flash convection zone leads to intershell dredge-up of additional carbon from the core into the intershell layer. Models that do not include overshoot at all convective boundaries (and include the partial mixing zone in a parametric way) feature neutron exposures that can explain only a small fraction of the observations. To explain the whole range of observational data, some spread in the efficiency of the neutron release is required in the scenario of $^{13}\text{C}(\alpha, n)$ occurring in the interpulse periods. If rotation is included, the s -process layer located at the core-envelope interface is continuously mixed throughout the interpulse period. The s -process layer is not stratified anymore, and the ^{13}C pocket that forms at the end of the third dredge-up is polluted with the ^{14}N from layers in the partial mixing zone with an initially larger H/ ^{12}C ratio. Using the mixing law from a stellar evolution sequence of an initially rapidly rotating star, the resulting neutron exposure is too small to allow any production of s -process elements.

We have constructed synthetic models with a parameterized range of mixing efficiencies during the interpulse phase. In these models we find a spread of neutron exposures in the s -process layer. Hence, we tentatively propose that the signature of rotationally induced mixing in AGB stars might be identified with the observationally inferred spread of neutron exposure in the interpulse. The spread of mixing efficiencies may be related to a spread of angular velocity gradients in stars of different initial rotational velocities,

masses, or evolutionary status. However, mixing efficiencies that would correspond to the observed spread of neutron exposures are substantially lower than the mixing law in our stellar evolution model with rotation. In this scenario this might be attributed to some effect of angular momentum redistribution and loss due to a physical process missing in our calculations, such as efficient third dredge-up, mass loss, and magnetic fields.

In the framework of the radiative interpulse s -process production site our simulations establish a relation between the intershell carbon abundance and the range of mixing efficiencies during the interpulse phase of AGB stars. Any mixing in the s -process layer during the interpulse phase and after the initial formation of the partial mixing zone can only reduce the final neutron exposure. A spectrum of slow-mixing efficiencies during the interpulse phase can deliver a spread in neutron exposures in accordance with the observed spread of s -process indices if the neutron exposure in the limiting case without mixing is larger than the largest observationally required neutron exposure (e.g., case ST $\times 2$ in Busso et al. 2001). If the carbon intershell abundance is larger than that obtained in models without hydrodynamic overshooting at the bottom of the He flash convection zone, then the ^{13}C abundance in the PM zone, and thus the neutron exposure, will be larger as well. As discussed in § 5.3, AGB models including this effect are in very good agreement with the observed carbon abundances of H-free and hot central stars of planetary nebulae, in which the progenitor AGB intershell abundance is believed to be seen at the surface.

In this paper we have used the nucleosynthesis and the observed features of the s -process to constrain stellar models. We have demonstrated how different mixing processes in different locations and at different times impact the current model of s -process nucleosynthesis in low-mass AGB stars. In the future we should improve the stellar physics in order to investigate which processes determine the mixing at the core-envelope interface and why mixing efficiencies in our rotating stellar model are not in agreement with the requirements of the s -process. The theory of angular momentum transport and loss may need to be revisited. The question of the third dredge-up in rotating-AGB stellar models needs additional consideration, and it is likely that the treatment of μ -gradients and their impact on mixing will play an important role.

F. H. appreciates support from D. A. Vandenberg through his Operating Grant from the Natural Science and Engineering Research Council of Canada. F. H. also thanks the Institute of Nuclear Theory at the University of Washington for its hospitality and the US Department of Energy for partial support during the completion of this work. The detailed and thoughtful comments by the referee have helped us to improve the presentation of this paper.

APPENDIX

DETAILS OF THE COMPUTATION OF [hs/l_s] AND s/s_{\odot} VERSUS τ

In § 2 we have presented an s -process calculation (Fig. 2) to establish the relation between the neutron exposure and the s -process indices [hs/l_s] and $\log(s/s_{\odot})$. We have used for this calculation initial mass fractions for the light neutron poison typically encountered in the partial mixing zone, including (^4He , ^{12}C , ^{16}O , ^{22}Ne) \simeq (0.74, 0.23, 0.01, 0.02). In our calculation the

temperature and density are chosen to be constant at $T = 9.8 \times 10^7$ K and $\rho = 2000$ g cm $^{-3}$. For intermediate- and heavy-mass isotopes, we have used an initial solar abundance distribution. The charged particle reactions listed in § 3 and neutron capture reactions on isotopes up to Pb are considered in the calculation. We have taken an initial mass fraction of ^{13}C of 0.03 and assumed only a residual amount of initial nitrogen [$X(^{14}\text{N}) = 1.2 \times 10^{-5}$]. The initial amount of protons was set to zero. With this choice a final neutron exposure of $\tau \simeq 0.7$ mbarn $^{-1}$ is reached when all ^{13}C is consumed.

In a partial mixing situation a significant amount of ^{14}N may be present. Because of different assumptions about mixing in the underlying stellar evolution model, the abundance of ^{12}C and ^{16}O may be different from model to model. The larger inter-shell ^{12}C abundance in models with hydrodynamic overshooting increases the neutron exposure that can be generated in the partial mixing zone (Lugaro et al. 2003b). However, we show here that the relation between τ and the s -process indices does not depend on the abundance distribution of light poison, for example, the presence of ^{14}N . We demonstrate this by some test calculations and by recalling some basic properties of the s -process as laid out in text books like Clayton (1968).

The neutron exposure is defined as $\tau = \int_0^t N_n v_T dt$, where N_n is the neutron density and v_T is the thermal velocity. The neutron density is related to the molar neutron abundance by $N_n = N_A \rho Y(n) A(n)$, where all symbols have their usual meaning. Since neutron captures are faster than any of the charged particle reactions, the neutron density is given by the ratio of neutron production by sources and destruction by sinks. The presence of light neutron poison (sinks) will depress the neutron density (and eventually the neutron exposure) and will thereby determine the amount of neutrons available to enter the s -process path. The s -process distribution (as given by the [hs/l s] index) as well as the total production of the s -process elements [as given by the index $\log(s/s_0)$] is then given by the number of neutrons that are captured by the s -process seed (usually ^{56}Fe) and other heavy elements. This number depends solely on the neutron density and the abundances and reaction rates of seed nuclei and all s -process species themselves. While neutron poison may limit the neutron density (and eventually τ), they cannot directly influence the relation of the integrated neutron density (τ) and the s -process distribution and total enhancement.

More specifically, the s -process distribution depends univocally on the number of neutrons, n_{56} , captured by ^{56}Fe and its progeny. If the abundance of ^{56}Fe is much larger than the abundance of its progeny, n_{56} is equal to the amount of ^{56}Fe destroyed by neutron captures:

$$Y(n_{56}) = -Y(^{56}\text{Fe}) = \int Y(^{56}\text{Fe}) Y(n) r_{56,(n,\gamma)} dt, \quad (\text{A1})$$

where $r_{56,(n,\gamma)}$ is the rate of the $^{56}\text{Fe}(n, \gamma)$ reaction and Y are molar abundances. If we assume $^{13}\text{C}(\alpha, n)$ to be the neutron source and $^{56}\text{Fe}(n, \gamma)$ and $^{14}\text{N}(n, p)$ to be the major neutron absorbers, then with the equilibrium condition $dN_n/dt = 0$ the total neutron abundance is given by

$$Y(n) = \frac{Y(^{13}\text{C}) Y(^4\text{He}) r_{13,(\alpha,n)}}{Y(^{14}\text{N}) r_{14,(n,p)} + Y(^{56}\text{Fe}) r_{56,(n,\gamma)}},$$

where $r_{14,(n,p)}$ is the rate of the $^{14}\text{N}(n, p)$ reaction and $r_{13,(\alpha,n)}$ is the rate of the $^{13}\text{C}(\alpha, n)$ reaction. The abundance of light neutron poison like ^{14}N determines the neutron density on which the number of neutron captures by ^{56}Fe and progeny depends (eq. [A1]). But the light neutron poison does not affect the relationship between $Y(n_{56})$ and $Y(n)$, i.e., between the s -process distribution and the neutron exposure.

In Figure 13 we show different cases of the same computation of Figure 2 performed with a range of initial ^{14}N mass fractions. Changing the initial mass fraction of ^{14}N leaves almost completely unchanged the relationship between the s -process distribution and the neutron exposure. The difference is in the final τ -value, which is much lower for a higher ^{14}N abundance.

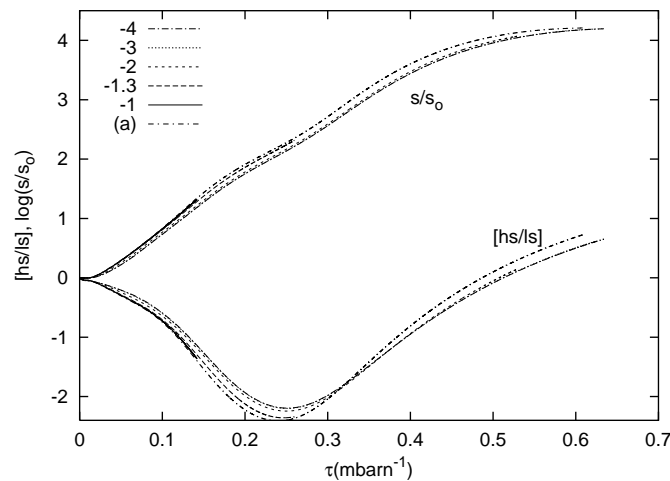


FIG. 13.—Same as Fig. 2, but each case with a different initial abundance of ^{14}N . The labels indicate the logarithm of the ^{14}N mass fraction. Case a has been computed with initial abundances $X(^4\text{He}) = 0.95$, $X(^{12}\text{C}) = 0.03$, $X(^{14}\text{N}) = 1.2 \times 10^{-5}$, and $\rho = 20$ g cm $^{-3}$.

TABLE 3
MAXIMUM τ AND (L/G) OBTAINED FOR DIFFERENT LOG D_{IP}

$\log D_{IP}$ ($\text{cm}^2 \text{s}^{-1}$)	τ (mbarn^{-1})	(L/G) Number Ratio
-0.0	0.12	4
-1.0	0.33	18
-2.0	0.64	55
No mixing	0.72	70

In the same way the relation of τ with the s -process indices is independent of the abundance of other light neutron sinks and rather general.

It follows that the parameter τ determines univocally the s -process distribution. Note that the conclusions reached in § 7 do not change if instead of τ we quantify the s -process with the parameter (L/G), which was introduced in § 4 and which is a measure of the number of neutrons captured by the heavy sink particle ^{63}G ; i.e., it is similar to considering the number of neutrons captured by ^{56}Fe . In the synthetic models presented in § 7 for a range of $\log D_{IP} \approx 0$ to -2 we obtain a range of τ and, correspondingly, a range of (L/G) (see Table 3).

REFERENCES

- Abia, C., Busso, M., Gallino, R., Domínguez, I., Straniero, O., & Isern, J. 2001, *ApJ*, 559, 1117
- Alongi, M., Bertelli, G., Bressan, A., & Chiosi, C. 1991, *A&A*, 244, 95
- Angulo, C., et al. 1999, *Nucl. Phys. A*, 656, 3
- Asida, S. M., & Arnett, D. 2000, *ApJ*, 545, 435
- Balick, B. 1987, *AJ*, 94, 671
- Bao, Z. Y., Beer, H., Käppeler, F., Voss, F., Wisshak, K., & Rauscher, T. 2000, *At. Data Nucl. Data Tables*, 76, 70
- Bergeron, P., Saffer, R. A., & Liebert, J. 1992, *ApJ*, 394, 228
- Busso, M., Gallino, R., Lambert, D. L., Travaglio, C., & Smith, V. V. 2001, *ApJ*, 557, 802
- Busso, M., Gallino, R., & Wasserburg, G. J. 1999, *ARA&A*, 37, 239
- Busso, M., Lambert, D. L., Beglio, L., Gallino, R., Raiteri, C. M., & Smith, V. V. 1995, *ApJ*, 446, 775
- Cameron, A. G. W. 1955, *ApJ*, 121, 144
- . 1960, *AJ*, 65, 485
- Caughlan, G. R., & Fowler, W. A. 1988, *At. Data Nucl. Data Tables*, 40, 283
- Clayton, D. D. 1968, *Principles of Stellar Evolution and Nucleosynthesis* (Chicago: Univ. Chicago Press)
- Cristallo, S., Straniero, O., Gallino, R., Herwig, F., Chieffi, A., Limongi, M., & Busso, M. 2001, *Nucl. Phys. A*, 688, 217
- Denissenkov, P. A., & Tout, C. A. 2003, *MNRAS*, 340, 722
- Despain, K. H. 1980, *ApJ*, 236, L165
- Deupree, R. G. 2000, *ApJ*, 543, 395
- Dinerstein, H. L. 2001, *ApJ*, 550, L223
- Dreizler, S., Werner, K., Heber, U., & Engels, D. 1996, *A&A*, 309, 820
- Feast, M. W. 1989, in *IAU Colloq. 106, Evolution of Peculiar Red Giant Stars*, ed. H. R. Johnson & B. Zuckerman (Cambridge: Cambridge Univ. Press), 26
- Freytag, B., Ludwig, H.-G., & Steffen, M. 1996, *A&A*, 313, 497
- Frogel, J. A., Mould, J., & Blanco, V. M. 1990, *ApJ*, 352, 96
- Funk, C., & Langanke, K. 1989, *ApJ*, 344, 46
- Gai, M., Keddy, R., Bromley, D., Olness, J., & Warburton, E. 1987, *Phys. Rev. C*, 36, 1256
- Gallino, R., Arlandini, C., Busso, M., Lugaro, M., Travaglio, C., Straniero, O., Chieffi, A., & Limongi, M. 1998, *ApJ*, 497, 388
- Gallino, R., Busso, M., & Lugaro, M. 1997, in *Astrophysical Implications of the Laboratory Study of Presolar Materials*, ed. T. Bernatowitz & E. Zinner (Woodbury: AIP), 115
- Gallino, R., Busso, M., Picchio, G., Raiteri, C. M., & Renzini, A. 1988, *ApJ*, 334, L45
- García-Segura, G., Langer, N., & Różycka, M. 1999, *ApJ*, 517, 767
- Gledenov, Y., Salatski, V., Sedyshev, P., Sedysheva, M., Koehler, P., Vesna, V., & Okunev, I. 1995, in *AIP Conf. Proc. 327, Nuclei in the Cosmos III*, ed. M. Busso, R. Gallino, & C. M. Raiteri (Woodbury: AIP), 173
- Goriely, S., & Mowlavi, N. 2000, *A&A*, 362, 599
- Greenstein, J. L. 1954, in *Modern Physics for Engineers*, ed. L. Ridenour (New York: McGraw-Hill), chap. 10
- Groenewegen, M. A. T., van den Hoek, L. B., & de Jong, T. 1995, *A&A*, 293, 381
- Hashimoto, M., Nomoto, K., Arai, K., & Kaminisi, K. 1986, *ApJ*, 307, 687
- Heger, A., Langer, N., & Woosley, S. E. 2000, *ApJ*, 528, 368
- Herwig, F. 2000, *A&A*, 360, 952
- . 2001, *Ap&SS*, 275, 15
- Herwig, F., Blöcker, T., & Driebe, T. 2000, *Mem. Soc. Astron. Italiana*, 71, 745
- Herwig, F., Blöcker, T., Langer, N., & Driebe, T. 1999, *A&A*, 349, L5
- Herwig, F., Blöcker, T., Schönberner, D., & El Eid, M. F. 1997, *A&A*, 324, L81
- Iben, I., Jr. 1975, *ApJ*, 196, 525
- Iben, I., Jr., & Renzini, A. 1982, *ApJ*, 263, L23
- Icke, V., Balick, B., & Frank, A. 1992, *A&A*, 253, 224
- Iliadis, C., D'Auria, J. M., Starrfield, S., Thompson, W. J., & Wiescher, M. 2001, *ApJS*, 134, 151
- Jorissen, A., & Arnould, M. 1989, *A&A*, 221, 161
- Jorissen, A., & Goriely, S. 2001, *Nucl. Phys. A*, 688, 508
- Jorissen, A., Smith, V. V., & Lambert, D. L. 1992, *A&A*, 261, 164
- Käppeler, F., Gallino, R., Busso, M., Picchio, G., & Raiteri, C. M. 1990, *ApJ*, 354, 630
- Koehler, P., Kavanagh, R., Vogelaar, R., Gledenov, Y., & Popov, Y. 1997, *Phys. Rev. C*, 56, 1138
- Koester, D., Weidemann, V., & Schulz, H. 1979, *A&A*, 76, 262
- Koesterke, L., & Hamann, W. R. 1997, *A&A*, 320, 91
- Kwok, S. 1982, *ApJ*, 258, 280
- Lambert, D. L., Smith, V. V., Busso, M., Gallino, R., & Straniero, O. 1995, *ApJ*, 450, 302
- Langer, N. 1998, *A&A*, 329, 551
- Langer, N., Heger, A., Wellstein, S., & Herwig, F. 1999, *A&A*, 346, L37
- Lugaro, M. 2001, Ph.D. thesis, Monash Univ., Australia
- Lugaro, M., Davis, A. M., Gallino, R., Pellin, M. J., Straniero, O., & Käppeler, F. 2003a, *ApJ*, 593, 486
- Lugaro, M., & Herwig, F. 2001, *Nucl. Phys. A*, 688, 201
- Lugaro, M., Herwig, F., Lattanzio, J. C., Gallino, R., & Straniero, O. 2003b, *ApJ*, 586, 1305
- Marigo, P., Bressan, A., & Chiosi, C. 1996, *A&A*, 313, 545
- Marigo, P., Girardi, L., & Bressan, A. 1999, *A&A*, 344, 123
- Mazzitelli, I., D'Antona, F., & Ventura, P. 1999, *A&A*, 348, 846
- McWilliam, A., & Lambert, D. L. 1988, *MNRAS*, 230, 573
- Melnick, G. J., Neufeld, D. A., Ford, K. E. S., Hollenbach, D. J., & Ashby, M. L. N. 2001, *Nature*, 412, 160
- Mowlavi, N. 1999, *A&A*, 344, 617
- Mowlavi, N., Jorissen, A., & Arnould, M. 1996, *A&A*, 311, 803
- Napiwotzki, R., Green, P. J., & Saffer, R. A. 1999, *ApJ*, 517, 399
- Nicolussi, G. K., Davis, A. M., Pellin, M. J., Lewis, R. S., Clayton, R. N., & Amari, S. 1997, *Science*, 277, 1281
- Nicolussi, G. K., Pellin, M. J., Lewis, R. S., Davis, A. M., Amari, S., & Clayton, R. N. 1998a, *Geochim. Cosmochim. Acta*, 62, 1093
- Nicolussi, G. K., Pellin, M. J., Lewis, R. S., Davis, A. M., Clayton, R. N., & Amari, S. 1998b, *Phys. Rev. Lett.*, 81, 3583
- Reimers, C., Dorfi, E. A., & Höfner, S. 2000, *A&A*, 354, 573
- Richer, H. B. 1981, *ApJ*, 243, 744
- Royer, F., Grenier, S., Baylac, M.-O., Gómez, A. E., & Zorec, J. 2002, *A&A*, 393, 897
- Royer, F., Zorec, J., & Frémat, Y. 2003, in *IAU Symp. 215, Stellar Rotation*, ed. A. Maeder & P. Eeens (ASP: San Francisco), in press
- Salasnich, B., Bressan, A., & Chiosi, C. 1999, *A&A*, 342, 131
- Savina, M. R., et al. 2003, *Geochim. Cosmochim. Acta*, in press
- Schaller, G., Schaerer, D., Meynet, G., & Maeder, A. 1992, *A&AS*, 96, 269
- Shaviv, G., & Salpeter, E. 1973, *ApJ*, 184, 191
- Skelton, R., Kavanagh, R., & Sargood, D. 1987, *Phys. Rev. C*, 35, 45
- Smith, V. V., & Lambert, D. L. 1986, *ApJ*, 311, 843
- Smith, V. V., Suntzeff, N. B., Cunha, K., Gallino, R., Busso, M., Lambert, D. L., & Straniero, O. 2000, *AJ*, 119, 1239
- Soker, N. 2001, *MNRAS*, 324, 699
- Spruit, H. C. 1998, *A&A*, 333, 603
- Stasińska, G., Górny, S. K., & Tylenda, R. 1997, *A&A*, 327, 736

- Straniero, O., Gallino, R., Busso, M., Chieffi, A., Raiteri, C. M., Salaris, M., & Limongi, M. 1995, *ApJ*, 440, L85
- Thielemann, F.-K., Arnould, M., & Truran, J. 1986, in *Advances in Nuclear Astrophysics*, ed. E. Vangioni-Flam (Gif-sur-Yvette: Editions Frontières), 525
- Truran, J. W., & Iben, I., Jr. 1977, *ApJ*, 216, 797
- Van Eck, S., Goriely, S., Jorissen, A., & Plez, B. 2003, *A&A*, 404, 291
- Van Winckel, H., & Reyniers, M. 2000, *A&A*, 354, 135
- Weidemann, V. 2000, *A&A*, 363, 647
- Weidemann, V., & Koester, D. 1984, *A&A*, 132, 195
- Wiescher, M., Goerres, J., & Thielemann, F.-K. 1990, *ApJ*, 363, 340
- Xiong, D. R. 1985, *A&A*, 150, 133
- Zinner, E. 1998, *Annu. Rev. Earth Planet. Sci.*, 26, 147